A New Class of Potent Vascular Endothelial Growth Factor Receptor Tyrosine Kinase Inhibitors: Structure−Activity Relationships for a Series of 9-Alkoxymethyl-12-(3-hydroxypropyl)indeno[2,1-*a*]pyrrolo[3,4-*c*]carbazole-5-ones and the Identification of CEP-5214 and Its Dimethylglycine Ester Prodrug Clinical Candidate CEP-7055

Diane E. Gingrich,[†] Dandu R. Reddy,[†] Mohamed A. Iqbal,[†] Jasbir Singh,[†] Lisa D. Aimone,[‡] Thelma S. Angeles,[§] Mark Albom,[§] Shi Yang,[§] Mark A. Ator,[§] Sheryl L. Meyer,[#] Candy Robinson,[||] Bruce A. Ruggeri,[||] Craig A. Dionne,[||] Jeffry L. Vaught,[⊥] John P. Mallamo,[†] and Robert L. Hudkins*[,†]

Departments of Medicinal Chemistry, Pharmacology, Biochemistry, Protein Expression, Oncology, and Discovery Research, Cephalon, Inc., 145 Brandywine Parkway, West Chester, Pennsylvania 19380

Received April 10, 2003

A series of potent vascular endothelial growth factor R2 (VEGF-R2) tyrosine kinase inhibitors from a new indenopyrrolocarbazole template is reported. The structure−activity relationships for a series of 9-alkoxymethyl-12-(3-hydroxypropyl)indeno[2,1-*a*]pyrrolo[3,4-*c*]carbazole-5-ones revealed an optimal R9 substitution with ethoxymethyl **19** (VEGF-R2 IC_{50} = 4 nM) and isopropoxymethyl **21** (VEGF-R2 IC_{50} = 8 nM) being the most potent inhibitors in the series. The VEGF-R2 activity was reduced appreciably by increasing the size of the R9 alkoxy group or by α-methyl branching adjacent to the ring. The combined R9 alkoxymethyl and N12 hydroxypropyl substitutions were required for potent VEGF-R2 activity, and the corresponding thioether analogues were weaker than their ether counterparts. Compound **21** (R9 isopropoxymethyl, CEP-5214) was identified as a potent, low-nanomolar pan inhibitor of human VEGF-R tyrosine kinases, displaying IC_{50} values of 16, 8, and 4 nM for VEGF-R1/FLT-1, VEGF-R2/KDR, and VEGF-R3/FLT-4, respectively, with cellular activity equivalent to the isolated enzyme activity. Compound **21** exhibited good selectivity against numerous tyrosine and serine/threonine kinases including PKC, Tie2, TrkA, CDK1, p38, JNK, and IRK. To increase water solubility and oral bioavailability, the *N*,*N*-dimethylglycine ester **40** was prepared. In pharmacokinetic studies in mice and rats, increased plasma levels of **21** were observed after oral administration of **40**. Compound **21** demonstrated significant in vivo antitumor activity in numerous tumor models and was advanced into phase I clinical trials as the water-soluble *N*,*N*-dimethylglycine ester prodrug **40** (CEP-7055).

Introduction

Angiogenesis, the generation and growth of new blood vessels from the endothelium of an existing vascular network, is an essential event in a variety of physiological and pathological processes.[1−3] Physiological conditions where angiogenesis occurs include embryogenesis, ovulation, and wound healing. Angiogenesis also occurs in pathological processes such as inflammation, retinopathies, rheumatoid arthritis, and psoriasis and is associated with tumor growth and the formation of metastases.[4−6]

Vascular endothelial growth factor (VEGF) is a key mediator of angiogenesis,[2,7] and evidence has accumulated that tumor VEGF expression is clinically associated with disease progression in a wide range of solid malignancies.[8] Virtually all cell types can express VEGF. Hypoxia and a variety of hormones, growth factors, cytokines, and oncogenes increase its expression.[7] VEGF drives the angiogenic cascade by promoting vascular endothelial cell expression of invasive proteases, activation of integrins, and the activation, proliferation, and migration of endothelial cells.[1−3,7] Two high-affinity VEGF transmembrane receptor tyrosine kinases, VEGF-R1 (Flt-1) and kinase insert domain-containing receptor VEGF-R2 (Flk-1, KDR), are expressed on vascular endothelial cells.[9] While VEGF-R1/Flt-1 is also expressed on nonendothelial cells (monocytes, dendritic cells, smooth muscle cells), VEGF-R2/KDR is primarily restricted to vascular endothelial cells and is the principal kinase receptor through which VEGFs exert their mitogenic, chemotactic, and vascular permeabilizing effects on the host vasculature.[9−11] A third homologous receptor, VEGF-R3 (Flt-4), is constitutively expressed on adult lymphatic endothelial cells and supports lymphangiogenesis.[12]

The enhanced expression of VEGF and VEGF-R2 on vascular endothelial cells during tumor angiogenesis on a variety of human and rodent tumors correlates with tumor growth rate, microvessel density and proliferation, and tumor metastatic potential.[1−6,13] The specificity of the receptor expression, the prerequisite of angio-

* To whom correspondence should be addressed. E-mail: rhudkins@cephalon.com. Phone: 610-738-6283. Fax: 610-738-6558.
[†] Department of Medicinal Chemistry.
[‡] Department of Pharmacology.
[§] Department of Biochemistry.
[#] Department of Protein Expression.
[||] Department of Oncology.
[⊥] Department of Discovery Research.

10.1021/jm0301641 CCC: $25.00
Published on Web 10/31/2003

Chart 1

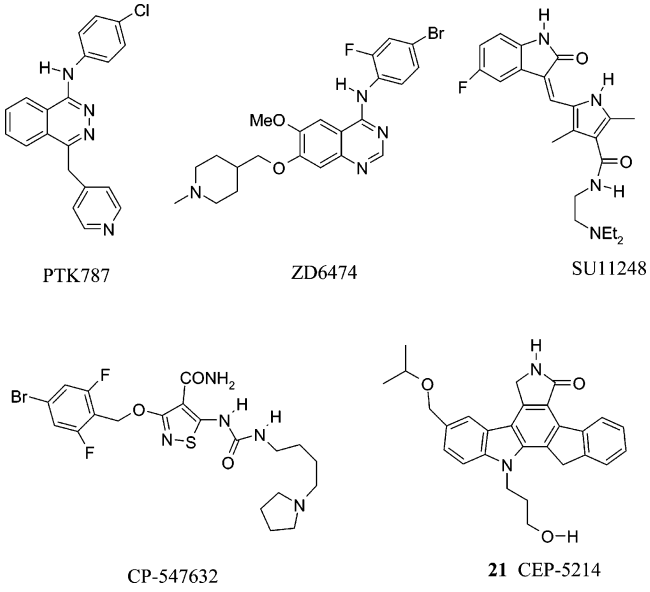

genesis for tumor growth, and the characteristic that the endothelium of normal mature cells remains generally quiescent makes disruption of the VEGF-R signaling pathway a highly attractive strategy for chronic oral therapy.

Antiangiogenesis therapies directed against VEGF-R kinases have been under active evaluation in clinical trials.[14,15] The preclinical profile has been reported for several orally active small-molecule inhibitors of VEGF-R kinases currently undergoing clinical evaluation, including PTK787[16] (phase III), ZD6474[17] (phase II), CP-547,632[18] (phase I/II), and SU-11248[14c] (phase I/II) (Chart 1). The Pfizer compound CP-547,632, an 11 nM inhibitor of VEGF-R2, is the first compound from a new series of isothiazoles. PTK787 (VEGF-R2 $IC_{50} = 37$ nM) is an anilinophthalazine derivative from Novartis. SU-11248 is the third indolinone to advance from Sugen/Pharmacia, and the AstraZeneca compound ZD6474 (VEGF-R2 $IC_{50} = 40$ nM) is an anilinoquinazoline. Indenopyrrolocarbazole CEP-5214 (**21**; VEGF-R2 $IC_{50} = 8$ nM) demonstrates significant in vivo antitumor activity in numerous tumor models, and the corresponding water-soluble *N*,*N*-dimethylglycine ester prodrug CEP-7055 (**40**) has advanced into phase I clinical trials.[19] We disclose here the synthesis and VEGF-R2 structure−activity relationships leading to the selection and advancement of CEP-5214 (**21**).

Chemistry

The compounds described were prepared starting from indenopyrrolocarbazole **1**.[20] The 5-oxo isomer **1** (6*H*,7*H*,12*H*,13*H*-indeno[2,1-*a*]pyrrolo[3,4-*c*]carbazole-5(5*H*)one) (Figure 1) was prepared as described previously utilizing a regioselective Diels−Alder reaction with 2-(2-indenyl)indole and ethyl *cis*-*β*-cyanoacrylate.[21] In the Diels−Alder step, the desired tetrahydrocarbazole diastereomer leading to **1** (Figure 1) was isolated, aromatized to the cyanoester carbazole, and subjected to a reductive cyclization to form the lactam (RaNi, H_2, DMF, MeOH). The 7-oxo regioisomer **1a** (Figure 1) was prepared in an analogous sequence after isolation of the

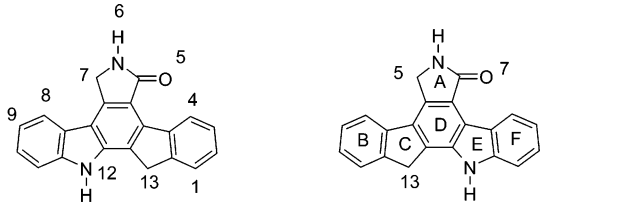

Figure 1. Structures of 5-oxo (**1**) and 7-oxo (**1a**) indenopyrrolocarbazoles.

Scheme 1[a]

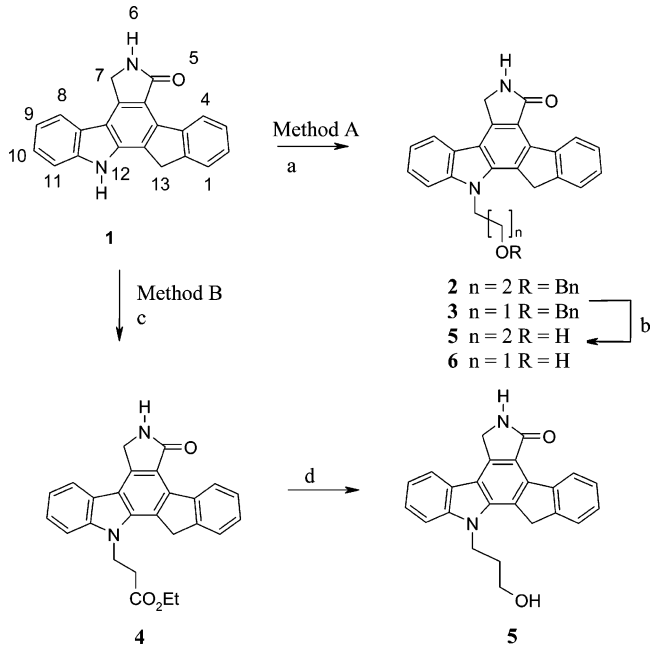

[a] Reagents and conditions: (a) NaH, $MsO(CH_2)_nOBn$, DMF, 90 °C; (b) 20% $Pd(OH)_2$−C, H_2, concentrated HCl, DMF; (c) $CH_2{=}CHCO_2Et$, DBU, CH_3CN, reflux; (d) $LiBH_4$, MeOH/THF, room temp.

tetrahydrocarbazole cyanoester regioisomer produced in the Diels−Alder reaction.[21] The N-substituted ethanol (**6**) and propanol (**5**) derivatives (Scheme 1, method B) were prepared from **1** by alkylation with the appropriate benzyl protected mesylate reagents (NaH, DMF). The benzyl protecting group was removed in high yield using 20% $Pd(OH)_2/H_2$ (Scheme 1, method A). A method to obtain larger quantities of propanol **5** utilized a heterogeneous Michael reaction of **1** with ethyl acrylate and DBU in acetonitrile to give ester **4**, followed by lithium borohydride reduction to alcohol **5** (Scheme 1, method B). Schemes 2 and 3 outline the routes to prepare the diol intermediates **8** and **16** required for the target ether and thioether analogues. Two methods were used to prepare the 9-hydroxymethyl intermediates (Scheme 2). In method A, formylation of **4** with α,α-dichloromethyl methyl ether[22] and tin(IV) chloride produced aldehyde **7** in 79% yield, which was reduced to **8** using lithium borohydride in a THF/methanol solution (96% yield). Scheme 2, method B, outlines a route to **8** using a palladium-catalyzed carbonylation sequence.[23] Protection of the lactam N−H was required to circumvent the major product being the reduced 9-H compound. The base stable dimethoxybenzhydryl group was used because of the ease of synthesis and the improved solubility in organic solvents, which aided purification. The

Scheme 2[a]

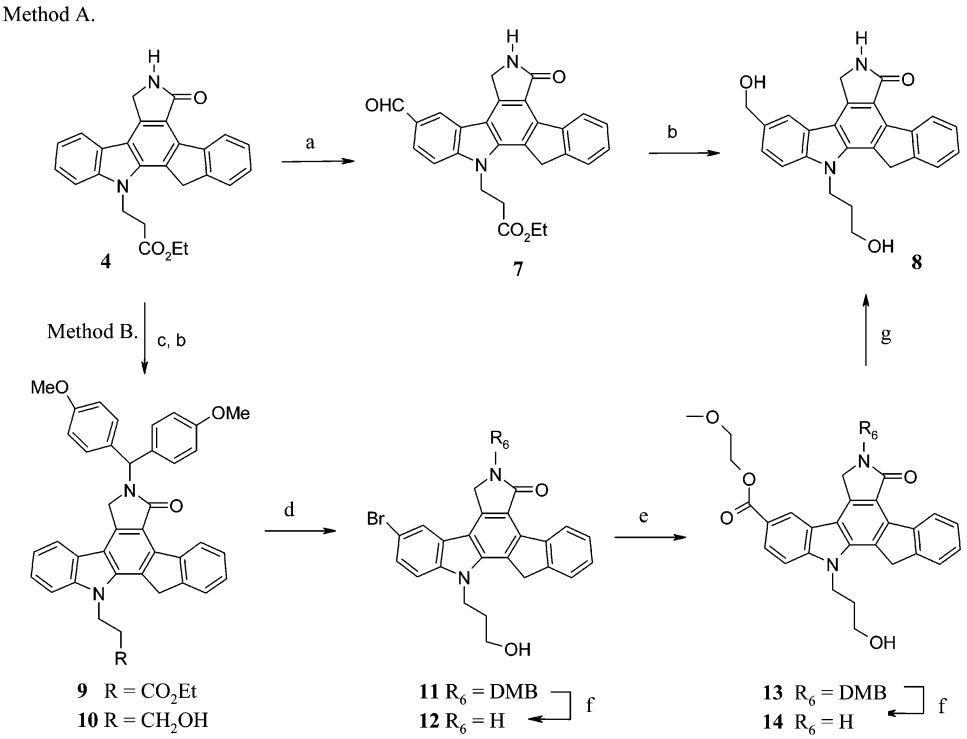

[a] Reagents and conditions: (a) Cl_2CHOCH_3, $SnCl_4$, CH_2Cl_2, $PhCH_3$; (b) $LiBH_4$, MeOH/THF, room temp; (c) 4,4′-dimethoxybenzhydrol, NMP, PhH, *p*-TsOH, reflux; (d) NBS, THF; (e) CO, $PdCl_2(PPh_3)_2$, NaOAc, $MeOCH_2CH_2OH$, 155 °C; (f) thioanisole, TFA, CH_2Cl_2; (g) DIBAL-H, CH_2Cl_2.

Scheme 3[a]

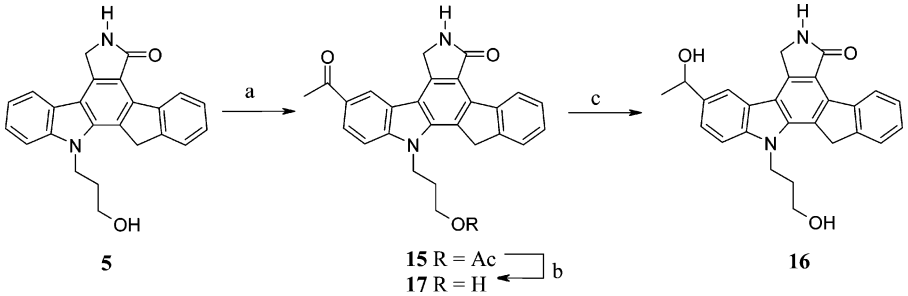

[a] Reagents and conditions: (a) CH_3COCl, $AlCl_3$, $C_2H_4Cl_2$, 0 °C to reflux; (b) K_2CO_3, MeOH/THF, room temp; (c) $LiBH_4$, THF, 0 °C to room temp.

bromoalcohol intermediate **11** (Scheme 2, method B) necessary for the carbonylation step was prepared by protection of ester **4** with 4,4′-dimethoxybenzhydrol (**9**) (NMP/benzene, *p*-TsOH), $LiBH_4$ reduction to propanol **10**, then regiospecific bromination using NBS in THF.[20] The reaction of **11**, carbon monoxide, and $PdCl_2(PPh_3)_2$ catalyst in methoxyethanol at 155 °C in a sealed tube produced the DMB protected methoxyethoxy ester **13** in 85% yield. Removal of the DMB group to **14** (TFA, anisole, methylene chloride) followed by diisobutylaluminum hydride reduction of the ester gave diol **8** (Scheme 2). Similarly, deprotection of DMB-**11** provided bromoalcohol **12**. Ether derivatives containing an α-methyl group adjacent to the ring were prepared from **16** (Scheme 3). Diol **16** was prepared by Friedel−Crafts acylation of **5** (acetyl chloride, $AlCl_3$) to give ketoester **15**, followed by lithium borohydride reduction to diol **16**, or removal of the acetate group to give ketoalcohol **17** (Scheme 3). 9-Carboxaldehyde **39** (Scheme 4) was prepared by first protecting **5** as the acetate (**39a**), formylation using α,α-dichloromethyl methyl ether and tin(IV) chloride to produce aldehyde **39b**, and then deprotection of the acetate using sodium methoxide in methanol. The 9-methyl-12-propanol derivative **41** was prepared from 9-hydroxymethyl **8** using TFAA and triethylsilane (Scheme 5).

The preferred approach to the target ethers and thioethers (Scheme 6) as outlined using diols **8** and **16** was to treat the pertrifluoroacetate intermediates (**8a**, **16a**) (trifluoroacetic anhydride, triethylamine) with an appropriate alcohol or thiol reagent. In cases where the N12 trifluoroacetate ester was isolated, treatment with lithium hydroxide in THF readily produced the desired target alcohol compound. Alternatively, the ether/thioether formation could be effected by directly treating the diol with camphor sulfonic acid in a solvent such as methylene chloride.[22] The dimethylglycine ester prodrug **40** was prepared by coupling **21** and *N*,*N*-dimethylglycine with 1-[3-(dimethylamino)propyl]-3-ethylcarbodiimide hydrochloride in DMA.

Scheme 4[a]

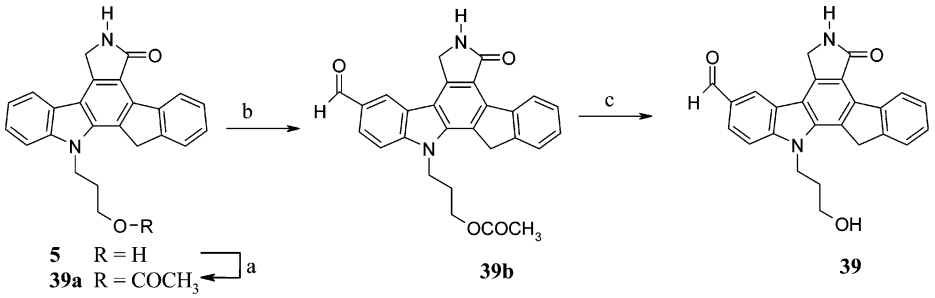

[a] Reagents and conditions: (a) Ac_2O, triethylamine, NMP, DMAP, room temp; (b) Cl_2CHOCH_3, $SnCl_4$, CH_2Cl_2, $PhCH_3$; (c) NaOMe, MeOH, NMP, room temp.

Scheme 5[a]

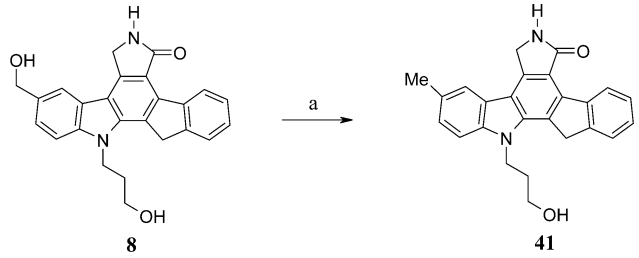

[a] Reagents and conditions: (a) trifluoroacetic anhydride, triethylsilane, CH_2Cl_2, 0 °C to room temp.

Results and Discussion

Inhibition of VEGF-R2 Receptor Tyrosine Kinase Activity in Vitro. The initial screening target for optimization of the indenopyrrolocarbazoles was inhibition of VEGF-R2 kinase activity. The VEGF-R2 assay utilized an enzyme linked immunosorbent assay (ELISA) based format[24] with time-resolved fluorescence readout and recombinant human phospholipase C-γ/glutathione S-transferase fusion protein as a substrate. The IC_{50} values reported are the average of two to three replications and are within 50% agreement. The VEGF-R2 inhibitory data are shown in Table 1. Novel heterocycles from our database were originally screened for VEGF-R2 activity, identifying the 5-oxo-indenopyrrolocarbazole **1** (Figure 1) as a potent VEGF-R2 lead with an IC_{50} of 110 nM. The 7-oxo regioisomer **1a** (Figure 1) was a weaker VEGF-R2 inhibitor (IC_{50} = 414 nM). Lead optimization of **1** was systematically conducted around the B- and F-rings, C13 indene, and the N12 positions (Figure 1). For brevity, the VEGF-R2 SAR of the 9-alkoxymethyl series and ensuing identification of the 9-isopropoxymethyl derivative (**21** CEP-5214) will be detailed. Substitutions at C13 and N6 were not favorable. A three-carbon alcohol at N12 was optimal because **5** displayed a VEGF-R2 IC_{50} of 48 nM. The ethanol derivative **6** was equally potent compared to the parent **1**. Exploring substitutions around the B-ring revealed the 9-position as the most favorable position for synthetic accessibility and enhancing VEGF-R2 potency. Thorough lead optimization of the R9 substituent was conducted on the N12-propanol lead **5**. Relative to **5**, compounds with 9-aldehyde (**39**) (105 nM), 9-methyl (**41**) (163 nM), 9-hydroxymethyl (**8**) (208 nM), 9-bromo (**12**) (104 nM), and 9-methyl ketone (**17**) (187 nM) substitutions tended to be weaker VEGF-R2 inhibitors. While the hydroxymethyl **8** was a relatively weak inhibitor with an IC_{50} of 208 nM, the methoxymethyl derivative **18** displayed a VEGF-R2 IC_{50} of 17 nM, 3-fold more potent than the lead **5** and 12-fold more potent than hydroxymethyl **8**. A number of analogues were prepared to study the SAR of methyl ether **18**. The ethyl ether derivative **19** was the most potent VEGF-R2 inhibitor in this series with an IC_{50} of 4 nM. Increasing the size of the alkoxy group to propyl (**20**, 13 nM) or butyl (**25**, 18 nM), while tolerated, did not further improve the potency. Branching was also explored on the methylene (benzyl) position and in the alkoxy moiety. An SAR observed with the size of the alkyloxy group indicated an optimum steric requirement in the lipophilic pocket at the R9 region. The isopropyl **21** (8 nM), *sec*-butyl **22** (12 nM), and *tert*-butyl **26** (11 nM) derivatives retained potent VEGF-R2 activity, while further increasing the alkyl length (for example, **27** and **28**) resulted in a decrease in activity. The stereochemistry in the alkyoxy portion did not appear critical because both enantiomers of **22** (**23** and **24**) displayed equivalent VEGF-R2 potency. However, α-methyl substitution adjacent to the carbazole ring as in **32** produced a 20-fold loss in VEGF-R2 activity compared to **19**. The more potent isomer **33** displayed an IC_{50} of 65 nM, while the IC_{50} of **34** was 240 nM (ER = 4). Compounds in the α-methyl series containing branched or larger alkyloxy groups, such as isopropoxy **36** and butyloxy **37**, were weak inhibitors of VEGF-R2.

The 9-isopropoxymethyl-12*H* analogue **38** (VEGF-R2 IC_{50} = 55 nM) demonstrated that both the R9 alkoxymethyl and N12 hydroxypropyl substitutions together are required for potent VEGF-R2 activity. The corresponding *N*-propanol thioether derivatives were prepared for comparison with the oxygen series. The ethylthiomethyl analogue **29** was about 5-fold weaker than the corresponding ethoxymethyl derivative **19**, and sulfur oxidation further decreased activity (compare **30** to **31**).

To assist in the design of indenopyrrolocarbazole inhibitors and support the SAR, an inhibitor binding model of VEGF-R2/KDR was built using the crystal structure of the tyrosine kinase domain of fibroblast growth factor receptor 1 as reported in complex with Su4984 (PDB code = 1AGW)[25] and the crystal structure of the human VEGF-R2/KDR kinase domain (PDB code = 1VR2).[26] The structures of a number of protein kinases in complex with ATP, or ATP analogues, have now been solved, which reveals the structural basis for nucleotide binding. For example, with cAMP-dependent protein kinase (PKA), the adenine moiety of ATP anchors to the linker region connecting the small

Scheme 6[a]

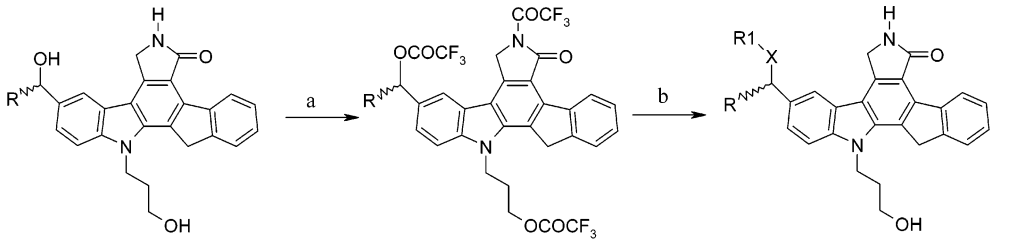

8 R = H
16 R = Me

8a R = H
16a R = Me

18-28 R = H; X = O
29-30 R = H; X = S
32,35-37 R = Me, X = O

[a] Reagents and conditions: (a) TFAA, triethylamine, CH_2Cl_2, 0 °C to room temp; (b) ROH or RSH, reflux.

Table 1. VEGF-R2 Kinase Activity of 9-Substituted 5-Oxo-indenopyrrolocarbazoles

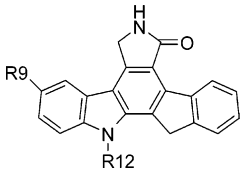

compd	R9	R12	VEGF-R2[a] IC_{50} (nM)
1	H	H	110
5	H	$CH_2CH_2CH_2OH$	48
6	H	CH_2CH_2OH	107
12	Br	$CH_2CH_2CH_2OH$	104
41	CH_3	$CH_2CH_2CH_2OH$	163
39	CHO	$CH_2CH_2CH_2OH$	105
17	$COCH_3$	$CH_2CH_2CH_2OH$	187
16	$CH(OH)CH_3$	$CH_2CH_2CH_2OH$	111
8	CH_2OH	$CH_2CH_2CH_2OH$	208
18	CH_2OCH_3	$CH_2CH_2CH_2OH$	17
19	$CH_2OCH_2CH_3$	$CH_2CH_2CH_2OH$	4
20	$CH_2OCH_2CH_2CH_3$	$CH_2CH_2CH_2OH$	13
21	$CH_2OCH(CH_3)_2$	$CH_2CH_2CH_2OH$	8
22	(±)-$CH_2OCH(CH_3)CH_2CH_3$	$CH_2CH_2CH_2OH$	12
23	(*S*)-$CH_2OCH(CH_3)CH_2CH_3$	$CH_2CH_2CH_2OH$	19
24	(*R*)-$CH_2OCH(CH_3)CH_2CH_3$	$CH_2CH_2CH_2OH$	12
25	$CH_2OCH_2CH_2CH_2CH_3$	$CH_2CH_2CH_2OH$	18
26	$CH_2OC(CH_3)_3$	$CH_2CH_2CH_2OH$	11
27	$CH_2OCH(CH_2CH_3)_2$	$CH_2CH_2CH_2OH$	35
28	$CH_2OCH_2CH_2CH(CH_3)_2$	$CH_2CH_2CH_2OH$	276
29	$CH_2SCH_2CH_3$	$CH_2CH_2CH_2OH$	21
30	$CH_2SCH(CH_3)_2$	$CH_2CH_2CH_2OH$	57
31	$CH_2SOCH(CH_3)_2$	$CH_2CH_2CH_2OH$	309
32	(±)-$CH(CH_3)OCH_2CH_3$	$CH_2CH_2CH_2OH$	83
33	(chiral)-$CH(CH_3)OCH_2CH_3$	$CH_2CH_2CH_2OH$	65
34	(chiral)-$CH(CH_3)OCH_2CH_3$	$CH_2CH_2CH_2OH$	240
35	(±)-$CH(CH_3)OCH_3$	$CH_2CH_2CH_2OH$	73
36	(±)-$CH(CH_3)OCH(CH_3)_2$	$CH_2CH_2CH_2OH$	411
37	(±)-$CH(CH_3)OCH_2CH_2CH_2CH_3$	$CH_2CH_2CH_2OH$	130
38	$CH_2OCH(CH_3)_2$	H	55
40	$CH_2OCH(CH_3)_2$	$CH_2CH_2CH_2OCOCH_2NMe_2$	18

[a] The VEGF-R2/KDR assay was conducted as described in the Experimental Section.

N-terminal and large C-terminal lobes via hydrogen bonds involving the N1 and N6 amino group with the backbone carbonyl of Glu121 and the amide NH of Val123.[27] The hydrogen-bond donor−acceptor pair of ATP binding to PKA is mimicked by the lactam NH and carbonyl of pyrrolocarbazole staurosporine (1STC). The VEGF-R2 cavity was identified using the coordinates for staurosporine and Su4984, known ATP-competitive inhibitors, and inhibitor **21** was docked using the FlexX module in Sybyl6.8 and minimized in the model. A binding mode including putative important interactions of **21** with VEGF-R2/KDR is shown in Figure 2. The proposed binding mode for **21** in this model is consistent with the lactam moiety of the indenopyrrolocarbazole mimicking the ATP donor−acceptor interactions, with lactam N−H sharing a hydrogen with Glu917 carbonyl and the lactam C═O hydrogen bonds with the backbone amide of Cys919. The R9 alkoxymethyl occupies a hydrophobic pocket, while the ether oxygen forms a significant hydrogen bond with Asp1046 and Lys868. The N-12 propyl alcohol forms key interactions with Arg1032 and Asn923. Compound **21** makes significant van der Waals contacts with the hydrophobic surface of the cleft: Val848, Leu1035, Cys1045, and Leu840. The decrease in activity of the α-methyl series can be predicted by the model, where the R-α-methyl isomer

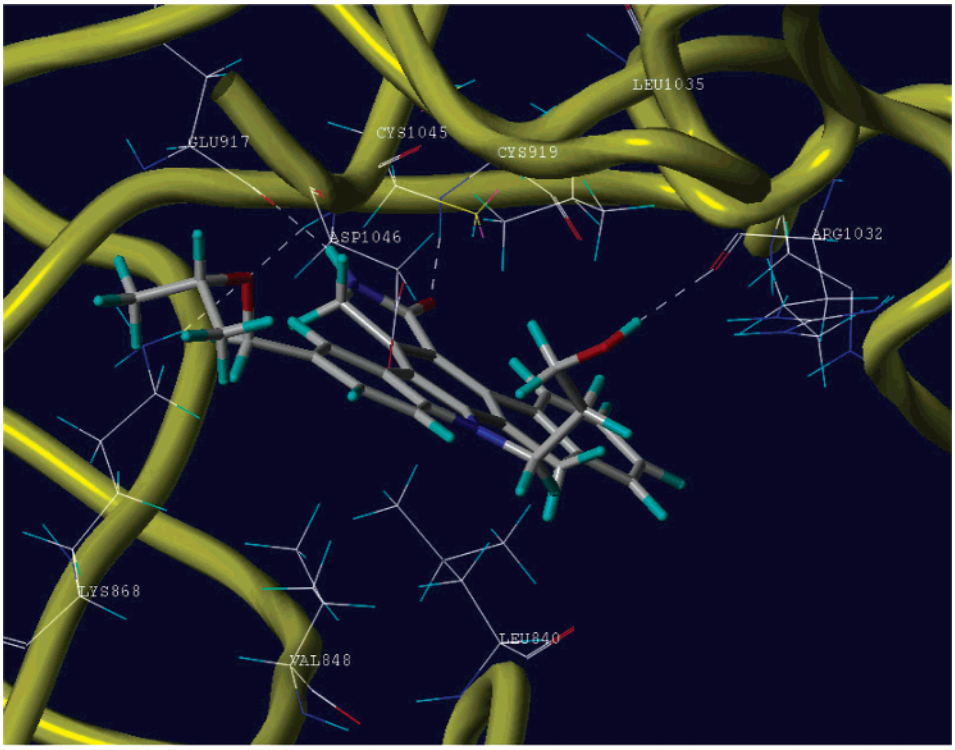

Figure 2. Important interactions of **21** with VEGF-R2/KDR tyrosine kinase.

Table 2. Inhibition of VEGF-Stimulated VEGF-R2 Autophosphorylation in HUVECs with Selected Indenopyrrolocarbazoles[a]

	concentration			
compd	10 nM	50 nM	100 nM	200 nM
19	3		4	
20				4
21	3		4	
23		4		
24		4		
25	0			4
26	4	4		
29				4
30				4
35	1		4	

[a] VEGF-R2/KDR autophosphorylation assay was conducted as described in the Experimental Section. Data were scored on the basis of a decrease in protein band density compared to that of VEGF-stimulated control (no inhibitor) as follows: 0 = no decrease; 1 = 1−25%; 2 = 26−50%; 3 = 51−75%; 4 = 76−100%.

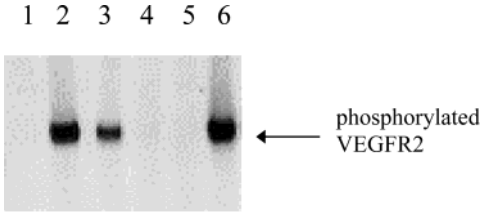

Figure 3. Inhibition of VEGF-stimulated VEGFR2 phosphorylation by compound **21** in HUVEC. Serum-starved HUVEC cells were incubated in the presence of DMSO (control) or different concentrations of **21** for 1 h at 37 °C prior to treatment with 10 ng/mL VEGF for 5 min. Immunoprecipitation was performed with anti-VEGFR peptide antibody from 1 mg of total protein. Separation was done on 6% Tris-glycine SDS−PAGE and probed with antiphosphotyrosine antibody. Detection was by enhanced chemiluminescence. Lane designations are as follows: (1) VEGF(−) control; (2) VEGF(+) control; (3) 10 nM **21**; (4) 100 nM **21**; (5) 1 μM **21**; (6) VEGF(+) control.

would be the more active enantiomer. The decrease in VEGF-R2 activity is most dramatic when comparing **21** (VEGF-R2 IC_{50} = 8 nM) to its α-methyl counterpart (±)-**36** (IC_{50} = 411 nM). The α-methyl group forces the bulky ^{i}PrO group to rotate above the 4-position to hydrogen-bond with Asp1046, resulting in unfavorable steric interactions with Val916, Leu889, and Phe1047.

Inhibition of VEGF-R2 Cell Activity in Vitro. The VEGF-R2 kinase inhibitory activity in cells was evaluated for dose-related inhibition of VEGF-R2/KDR autophosphorylation utilizing human umbilical vein endothelial cells (HUVECs) monitoring inhibition of VEGF-induced stimulation of VEGF-R2/KDR phosphorylation. Inhibitors from Table 2 screened in HUVECs at concentrations of 100 nM or lower (compounds **19**, **21**, **23**, **24**, **26**, **35**) gave complete inhibition of VEGF-stimulated VEGF-R2 phosphorylation in both the human (HUVECs) and murine (SVR data not shown) endothelial cells in vitro. The cellular IC_{50} for compound **21** was estimated to be ≃10 nM in HUVECs (Figure 3), indicating that the compound is highly cell-permeable and closely comparable to an IC_{50} of 8 nM in the isolated VEGF-R2 kinase assay. A time course study revealed that the inhibitory activity of **21** on VEGF-R2/KDR receptor phosphorylation in murine and human endothelial cells was observed within 15 min of exposure to cells. In a washout assay conducted to determine the duration of inhibitory effects of **21** on VEGF-stimulated VEGF-R2 phosphorylation, inhibition was sustained maximally for 1 h, was apparent for 3 h following washout, and then declined to basal levels by 6 h, consistent with competitive and reversible inhibition of VEGF-R2/KDR kinase activity in cells as was observed in the human VEGF-R2 kinase assay.

Prodrug for Oral Administration of Compound 21 (CEP-5214). The pharmacokinetics of compounds **19** and **21** were studied in vivo in rats and in vitro in rat

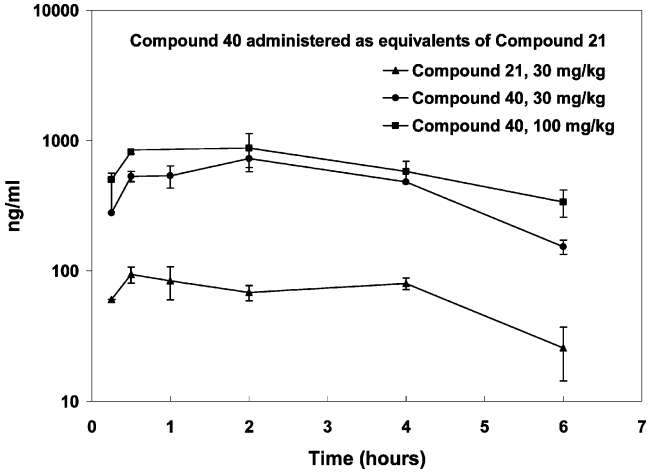

Figure 4. Plasma levels of compound **21** (ng/mL) in rat, administered as prodrug **40** (30 and 100 mg/kg) or parent **21** (30 mg/kg).

Scheme 7[a]

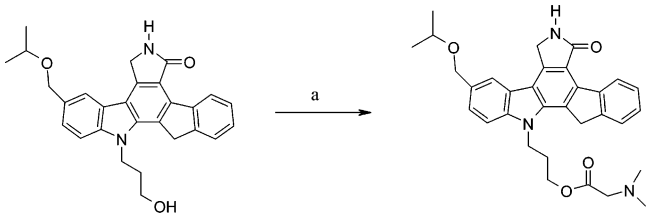

21 CEP-5214 **40** CEP-7055

[a] Reagents and conditions: (a) *N*,*N*-dimethylglycine, EDCI, DMAP, DMA, 35−45 °C, 2 h.

liver S9 fraction for stability. An important objective was to establish the metabolic stability of the benzylic ether linkage in vitro. In the rat liver S9 fraction, on the basis of mass spectral analysis after 2 h of incubation, 98% of the branched isopropoxy compound **21** remained intact in the absence of NADPH and 46% remained intact in the presence of NADPH cofactor. The ethoxy compound **19** was unstable in the S9 preparation in the absence or presence of NADPH cofactor, showing 0% and 2% remaining after a similar incubation period. Oral dosing of **21** at 30 mg/kg to rats showed maximum plasma levels of about 100 ng/mL (Figure 4). The low aqueous solubility (10 μg/mL) was believed to be a reason for the low oral bioavailability. Extensive evaluations of different formulations for **21** in an attempt to improve the oral bioavailability and increase the drug plasma levels at high doses for toxicity studies were unsuccessful. Therefore, to increase the aqueous solubility of **21**, a series of prodrug esters[28] were prepared and screened for solubility and stability. The *N*,*N*-dimethylglycine ester **40** (Scheme 7) as the hydrochloride showed good solubility in water (40 mg/mL) and the free base was readily soluble and stable as a 1% aqueous acetic acid solution, allowing for parenteral or oral administration. Pharmacokinetic studies in rats and nude mice demonstrated that following oral administration of **40**, only **21** was detected in the plasma compartment; no **40** was detected within the shortest time frame (∼5 min postdosing) evaluated. Moreover, oral administration of **40** produced better systemic exposure compared to **21** (Figure 4) at all doses. The oral bioavailability of **40** in nude mice (measured as **21** in plasma) was ∼15%, comparable to that observed in CD-1 mice, and was ∼20% in rats. In nude mice, plasma levels of **21** were dose-proportional between 3.6 and 11.9 mg/kg of orally administered **40** with C_{max} plasma levels of about 100 ng/mL achieved.[29] While cleavage in plasma cannot be ruled out, it is believed that the prodrug ester is converted primarily in the stomach. A manuscript is in preparation describing the optimization, solubility, and prodrug stability leading to the selection of ester **40** (CEP-7055) for advancement as a water-soluble form of **21**.

Table 3. Kinase Inhibitory Profile of **21**

	kinase IC_{50} (nM) (av ± SD)
VEGF-R1	16 ± 1
VEGF-R2	8 ± 2
VEGF-R3	4 ± 2
Tie2	>10000
Flt3	1.6 ± 0.7
FGF-R1	162 ± 37
PDGF-Rβ	406 ± 76
Kit	57 ± 5
TrkA	>3000
βIrk	>10000
JNK1β1	448 ± 102
CHK1	>3000
CDS1	>3000
Cdk1/cyclinB	>10000
rat brain PKC (α, β, γ isozymes)	>10000
p38α	>10000

Kinase Selectivity Profile for CEP-5214 (21). The inhibitory profile of **21** was subsequently determined in a panel of in vitro kinase enzyme assays and is shown in Table 3. As previously described, **21** is a potent, low nanomolar inhibitor of the primary screening target, human VEGF-R2 tyrosine kinase. It was also discovered to be a potent, low nanomolar pan inhibitor of the human VEGF-R tyrosine kinase family, displaying IC_{50} values of 16, 8, and 4 nM for VEGF-R1/Flt-1, VEGF-R2/KDR, and VEGF-R3/Flt-4, respectively. The Hill slopes of **21** for human VEGF-R2/KDR kinase approached unity. ATP competition studies confirmed competitive binding. Compound **21** demonstrated weaker inhibitions of the human c-Kit, PDGF-Rβ, JNK1β1, and FGF-R1 kinases, with IC_{50} values of 57, 406, 448, and 162 nM, respectively, and was a potent inhibitor of Flt3 kinase with an IC_{50} value of 1.6 nM. Compound **21** was weak to inactive against the additional tyrosine and serine/threonine kinases evaluated, including PKC, Tie2, TrkA, CDK1, p38, and IRK (Table 3). Of the VEGF-R2 inhibitors currently undergoing clinical evaluation, compound **21** is the most potent pan inhibitor of the human VEGF-R tyrosine kinase family members. The Pfizer compound CP-547,632, SU-11248 (Sugen/Pharmacia), and the AstraZeneca compound ZD6474 are selective for VEGF-R2. The Novartis compound PTK787, a 37 nM VEGF-R2 inhibitor, is about 2-fold selective over VEGF-R1.

In Vitro Antiangiogenesis Activity. On the basis of its potent and selective inhibition of the VEGF-R kinases and marked inhibition of VEGF-R2 phosphorylation in human and rodent endothelial cells, compound **21** was evaluated in in vitro and ex vivo bioassays of angiogenesis. The rat aortic ring explant model in three-dimensional collagen gel matrixes and the HUVEC

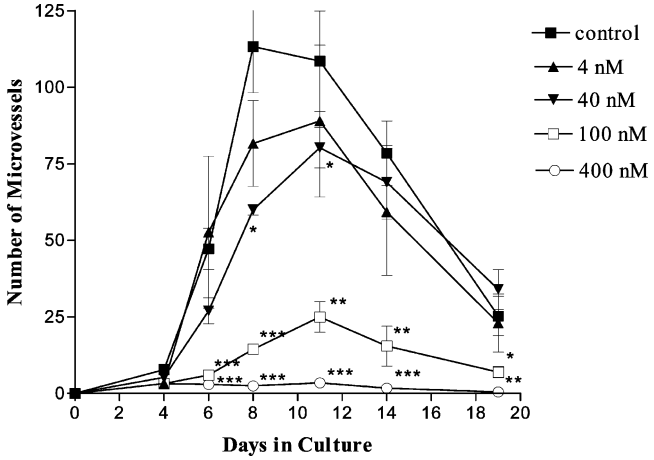

Figure 5. Dose-related effects of **21** on VEGF-stimulated microvessel growth in rat aortic ring collagen gel explant cultures. Shown is the effect of increasing concentrations of VEGFR kinase inhibitor **21** on angiogenesis in serum-free collagen gel cultures of rat aortic ring explants maintained in serum-free MCDB 131 medium. Aortic rings were stimulated with 4 ng/mL recombinant murine VEGF for 24 h prior to the addition of compound. Values are the mean ± SE of microvessel outgrowths, $n = 3$ per time point. (∗) $p < 0.05$; (∗∗) $p < 0.01$; (∗∗∗) $p < 0.01$. The p values are relative to untreated controls by the Student−Newman−Keuls method.

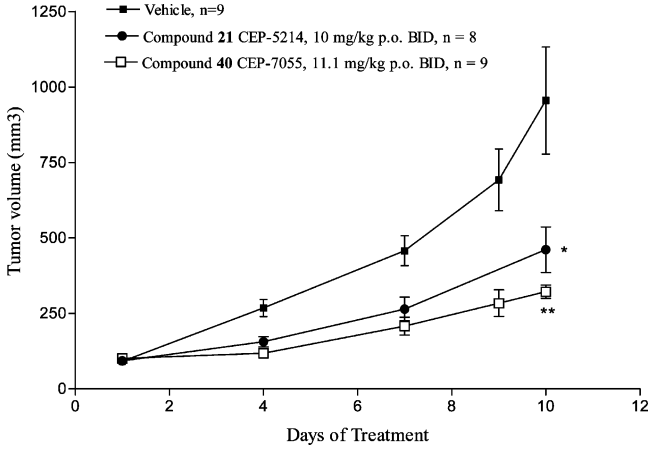

Figure 6. Effect of **21** and prodrug **40** on the growth of SVR angiosarcoma xenografts in nude mice. Murine endothelial SVR cells (1 × 106) were injected into the right flank of female BALB/c nude mice. At day 6 postimplantation when palpable tumors were confirmed, mice were randomized into vehicle and treatment groups ($n = 8$ or 9) and the compounds were administered at the specified concentration, orally, twice a day. Statistical analyses were done using the Mann−Whitney sum test: (∗) $p < 0.05$; (∗∗) $p < 0.01$.

capillary tube formation assay on a Matrigel synthetic basement membrane matrix are two widely used ex vivo and in vitro angiogenesis systems.[30] Both assays are sensitive to the angiogenic effects of VEGF and to VEGF-R2 inhibitors. Compound **21** displayed statistically significant dose-related inhibition of complete HUVEC capillary tube formation in the absence of apparent endothelial cell cytotoxicity. Compound **21** inhibited VEGF-induced capillary tube formation by 21% (40 nM), 75% (100 nM), and 89% (400 nM), respectively. The antiangiogenic response to **21** was further evaluated ex vivo in rat aortic ring explant cultures over a 19-day time course in the presence of exogenous VEGF stimulation, where dose-related inhibitory effects on microvessel growth were observed from 4 to 400 nM (Figure 5). At days 8 and 11, when microvessel growth was at its peak in control cultures, statistically significant effects were observed at 40 nM of **21**. Concentrations of 100 and 400 nM significantly inhibited vessel outgrowth relative to near controls in the absence of apparent cytotoxicity in the primary aortic ring explants.

In Vivo Antitumor Activity. Detailed oral antitumor efficacy of **21** or the prodrug **40** in a variety of established murine and human tumor models in nude mice along with the pharmacokinetics of **40** in nude mice is reported elsewhere.[29,31] The antitumor activity of the indenopyrrolocarbazole compounds reported here were routinely evaluated using the SVR murine angiosarcoma xenograft model.[32] Compound **21** administered orally (Figure 6) at a dose of 10 mg/kg b.i.d. resulted in significant inhibition of SVR tumor growth relative to vehicle-treated controls as early as day 4 of dosing and extending to day 10, with a maximum inhibition of 57% ± 5%. A comparable effect was observed with prodrug **40** at the equivalent dose of **21**. In multiple, independent experiments, no toxicity or morbidity was observed. The minimum effective dose (MED) for consistent and significant inhibition of **21** in this murine SVR angiosarcoma xenograft model was 1−3 mg/kg b.i.d. administered over a 10-day dosing regimen. The maximum efficacy achieved in this model was ∼70% inhibition of tumor growth at a dose of 23.8 mg/kg b.i.d. (equivalent to 20 mg/kg **21**) of **40**. No deaths occurred at the high dose. Results of antitumor efficacy after longer dosing in multiple tumor models have been reported.[31]

Conclusions

Potent VEGF-R2 tyrosine kinase inhibitors from a new indenopyrrolocarbazole template are reported. The structure−activity relationships revealed a size requirement in the R9 pocket with the ethoxymethyl (**19**) and isopropoxymethyl (**21**) being the most potent inhibitors from the series. Increasing the alkyl size at R9 or α-methyl branching adjacent to the ring significantly reduced VEGF-R2 activity in this series. The ether series was more potent for VEGF-R2 than the corresponding sulfur analogues. In addition, both the R9 alkoxymethyl and N12 hydroxypropyl substitutions together were required for potent VEGF-R2 activity. An important characteristic of this series was that several compounds, including **19**, **21**, **23**, **24**, and **26**, displayed activity in cells approximately equivalent to their isolated enzyme IC_{50} values. Compound **21** (CEP-5214) was also a potent, pan inhibitor of the human VEGF-R tyrosine kinase family, displaying comparable IC_{50} values for VEGF-R1, VEGF-R2, and VEGF-R3. Compound **21** demonstrated selectivity against a number of tyrosine and serine/threonine kinases including PKC, Tie2, TrkA, CDK1, p38, and IRK. To increase water solubility, the *N*,*N*-dimethylglycine ester **40** was prepared. In pharmacokinetic studies in mice and rats, increased plasma levels of **21** were observed after oral administration of **40**. Compound **21** demonstrated significant in vivo antitumor activity at relevant oral doses and has advanced into phase I clinical trials as the water-soluble *N*,*N*-dimethylglycine ester prodrug **40**.

Experimental Section

Chemistry. All reagents and solvents were obtained from commercial sources and used as received. The ^{1}H NMR spectra were recorded at 300 or 400 MHz in the solvent indicated with tetramethylsilane as an internal standard. Coupling constants (*J*) are given in hertz (Hz). Analytical HPLC purity was carried out on a Zorbax RX8, 5 mm × 150 mm, with product eluted with a mixture of acetonitrile and water containing 0.1% trifluroacetic acid with a gradient of 10−100% and a flow rate of 1 mL/min over 20 min. Column chromatography was performed on silica gel 60 (230−400 mesh). M-Scan Inc., West Chester, PA, performed high-resolution mass spectra (FAB).

12-(3-Benzyloxypropyl)-6*H*,7*H*,13*H*−indeno[2,1-*a*]pyrrolo[3,4-*c*]carbazole-5-one (2). Method A. To a solution of **1** (1.0 g, 3.2 mmol) in dry DMF (60 mL) was added solid NaH (60%, 130 mg, 3.2 mmol) at room temperature. After the mixture was stirred for 30 min, 2-benzyloxypropyl methanesulfonate was added (828 mg, 3.4 mmol), followed by heating at 90 °C for 4 h. The solution was cooled to room temperature and the DMF was removed at reduced pressure to leave a semisolid. Ethyl acetate (100 mL) was added and the resulting suspension was stirred and collected to give 1.2 g (82%) of **2** as a yellowish solid. ^{1}H NMR (DMSO-d_6): δ 2.09 (m, 2H), 3.54 (m, 2H), 4.45 (s, 2H), 4.51 (s, 2H), 4.82 (m, 2H), 4.93 (s, 2H), 7.30−7.53 (m, 10H), 7.73 (d, 1H, J = 8 Hz), 8.01 (d, 1H, J = 8 Hz), 8.59 (s, 1H), 9.50 (d, 1H, J = 7.5 Hz). MS (*m*/*z*): 459 (M + 1).

12-(3-Hydroxypropyl)-6*H*,7*H*,13*H*-indeno[2,1-*a*]pyrrolo-[3,4-*c*]carbazole-5-one (5). A solution of **2** (1.0 g, 2.2 mmol), 20% $Pd(OH)_2$ (200 mg), and concentrated HCl (3 drops) in DMF (100 mL) was hydrogenated on a Parr apparatus for 14 h. The catalyst was removed by filtration through Celite and the solvent was concentrated at reduced pressure to leave a solid that was triturated with methanol, collected, and dried to give 700 mg (86%, 96% purity) of **5** as a white solid, mp 280−284 °C (dec). ^{1}H NMR (DMSO-d_6): δ 1.96 (m, 2H), 3.52 (m, 2H), 4.57 (s, 2H), 4.78 (m, 2H), 4.95 (s, 2H), 7.30−7.46 (m, 3H), 7.55 (m, 2H), 7.67 (d, 1H, J = 8 Hz), 7.75 (d, 1H, J = 8 Hz), 8.0 (d, 1H, J = 8 Hz), 8.60 (s, 1H), 9.51 (d, 1H, J = 7.5 Hz). MS (*m*/*z*): 369 (M + 1).

Method B. To a suspension of **1** (8.0 g, 25.8 mmol) in acetonitrile (300 mL) was added ethyl acrylate (4.19 mL, 38.7 mmol) followed by 1,8-diazabicyclo[5.4.0]undec-7-ene (DBU) (1.93 mL, 0.013 mmol) under a nitrogen atmosphere. The heterogeneous reaction mixture was heated to reflux for 18 h, then cooled to room temperature. The solid was collected by filtration, washed with acetonitrile, and dried to yield 5.4 g (78%) of **4**. ^{1}H NMR (DMSO-d_6): δ 9.72 (t, 3H, J = 6. 8 Hz), 2.87 (m, 2H), 3.89 (q, 2H, J = 6.8 Hz), 4.49 (s, 2H), 4.88 (s, 2H), 4.92 (m, 2H), 7.29−7.48 (m, 3H), 7.50−7.73 (m, 3H), 7.96 (d, 1H, J = 7.3 Hz), 8.56 (s, 1H), 9.47 (d, 1H, J = 7.3 Hz). MS (*m*/*z*): 411 (M + 1). To a stirred solution **4** (1.0 g, 2.4 mmol) in THF/methanol (150 mL, 4:1) was added lithium borohydride (7.2 mL of 2 M solution in THF). The mixture was stirred overnight. Then the reaction was quenched by addition of 2 N HCL (15 mL), the mixture was diluted with an equal volume of water, and the product **5** was collected and dried to give 760 mg (86%). Compound **5** prepared by method B showed physical and spectral characteristics identical to those prepared by method A.

12-(2-Benzyloxyethyl)-6*H*,7*H*,13*H*-indeno[2,1-*a*]pyrrolo-[3,4-*c*]carbazole-5-one (6). This compound was prepared by the same general procedure as for **5** (method A). Intermediate **3** was prepared by alkylation of **1** with 2-benzyloxyethyl methanesulfonate. MS (*m*/*z*): 445 (M + 1). ^{1}H NMR (DMSO-d_6): δ 3.58 (m, 2H), 4.48 (s, 2H), 4.51 (s, 2H), 4.80 (m, 2H), 4.95 (s, 2H), 7.30−7.58 (m, 10H), 7.75 (d, 1H, J = 8 Hz), 8.00 (d, 1H, J = 8 Hz), 8.6 (s, 1H), 9.50 (d, 1H, J = 7.5 Hz). Intermediate **3** was deprotected using 20% $Pd(OH)_2$ (100 mg) and concentrated HCl (3 drops) in DMF (60 mL). Compound **6** (85% yield, 97% purity): mp >300 °C. ^{1}H NMR (DMSO-d_6): δ 3.8−3.9 (b, 2H), 4.55 (s, 2H), 4.77 (t, 2H), 4.9 (s, 2H), 5.0 (b, 1H, D_2O exchange), 7.3−7.45 (m, 3H), 7.5−7.57 (t, 1H), 7.67 (d, 1H, J = 6 Hz), 7.5 (d, 1H, J = 6 Hz), 8.0 (d, 1H, J = 6 Hz), 8.57 (s, 1H), 9.5 (d, 1H, J = 7 Hz). MS (*m*/*z*): 355 (M + 1).

9-Hydroxymethyl-12-(3-hydroxypropyl)-6*H*,7*H*,13*H*-indeno[2,1-*a*]pyrrolo[3,4-*c*]carbazole-5-one (8). Method A. To a stirred suspension of ester **4** (10 g, 24.3 mmol) and 1,1-dichloromethyl methyl ether (55.6 g, 488 mmol) in methylene chloride (250 mL) and toluene (40 mL) was added tin(IV) chloride (95.1 g, 365 mmol) (1 M solution in methylene chloride). After 4.5 h at room temperature, the reaction was quenched with aqueous 2 N HCl (150 mL) and the methylene chloride/toluene layer was removed under vacuum. To the crude residue, 2 N HCl (350 mL) and *tert*-butyl methyl ether (200 mL) were added. The suspension was stirred at room temperature for 14 h, collected, washed with *tert*-butyl methyl ether, and then resuspended in ethyl acetate/tetrahydrofuran (1:1; 250 mL) and stirred for 14 h at room temperature. The solid was collected, washed with cold ethyl acetate, and dried to give 8.4 g (79% yield, 99% purity) of compound **7**. ^{1}H NMR (DMSO-d_6): δ 0.98 (t, 3H), 2.92 (t, 2H), 3.88 (q, 2H), 4.65 (s, 2H), 4.92−5.08 (m, 4H), 7.25−7.45 (m, 2H), 7.75 (d, 1H), 7.85 (d,1H), 8.05 (d, 1H), 8.52 (s, 1H), 8.69 (s, 1H), 8.95 (s, 1H), 10.18 (s, 1H). MS (*m*/*z*): 439 (M + 1). To a suspension of intermediate **7** (2.4 g, 5 mmol) in THF (50 mL) at 0 °C under nitrogen was added lithium borohydride (25 mL of 2 M solution in THF). The reaction mixture was stirred for 3.5 h at room temperature and cooled to 0 °C, and methanol was added slowly until no evolution of gas was observed. The mixture was concentrated at reduced pressure to give a yellow solid, which was triturated with water and ether, collected by filtration, and dried to yield 2.0 g (96%, purity 96.5%) of diol **8**. ^{1}H NMR (DMSO-d_6): δ 1.92 (m, 2H), 3.46 (m, 2H), 4.50 (s, 2H), 4.65 (s, 2H), 4.71 (m, 2H), 4.88 (s, 2H), 7.32−7.39 (m, 2H), 7.47 (d, 1H, J = 8.3 Hz), 7.65 (m, 2H), 7.89 (s, 1H), 8.53 (s, 1H), 9.46 (d, 1H, J = 7.4 Hz). MS (*m*/*z*): 399 (M + 1). HRMS (FAB) calcd for $C_{25}H_{22}N_2O_3$: 399.1708; found 399.1709.

Diol 8. Method B. To a suspension of ester **4** (5.62 g, 13.7 mmol) in benzene (300 mL) and *N*-methylpyrrolidine (60 mL) at room temperature under nitrogen was added *p*-toluenesulfonic acid monohydrate (2.48 g, 13.0 mmol) and 4,4′-dimethoxybenzhydrol (3.19 g, 13.0 mmol). The mixture was heated to reflux for 8 h, cooled to room temperature, and diluted with ethyl acetate (300 mL). The ethyl acetate layer was washed with a saturated sodium bicarbonate solution, water, and brine and then dried over magnesium sulfate. The drying agent was removed by filtration and the solvent was concentrated to give 8.31 g (95%) of intermediate **9** as an orange solid. ^{1}H NMR ($CDCl_3$): δ 1.18 (t, 3H, J = 7.1 Hz), 2.84 (m, 2H), 3.80 (6H, s), 4.12 (q, 2H, J = 7.1 Hz), 4.38 (s, 2H), 4.72 (2H, s), 4.94 (m, 2H), 6.90 (d, 4H, J = 8.5 Hz), 6.96 (s, 1H), 7.26 (d, 4H, J = 8.5 Hz), 7.34−7.49 (m, 5H), 7.61 (d, 1H, J = 7.4 Hz), 7.69 (d, 1H, J = 7.7 Hz), 9.65 (d, 1H, J = 7.8 Hz).

To a stirred solution of intermediate **9** (7.8 g, 12.2 mmol) in THF (480 mL) and methanol (93 mL) was added lithium borohydride (18.9 mL of a 2.0 M solution in THF) dropwise. The reaction was monitored by HPLC until completion, the mixture was cooled on an ice bath, and the reaction was then quenched with 2 N HCl (60 mL). Water (750 mL) was added to the mixture and the precipitate was collected by filtration and dried to give 7.2 g (99%) of **10** as white solid. ^{1}H NMR (DMSO-d_6): δ 1.93 (m, 2H), 3.66 (m, 2H), 3.71 (s, 6H), 4.55 (s, 2H), 4.73 (m, 2H), 4.79 (s, 2H), 6.70 (s, 1H), 6.93 (d, 4H, J = 8.44 Hz), 7.22 (d, 4H, J = 8.4 Hz), 7.26 (m, 1H), 7.34−7.46 (m, 2H), 7.49 (m, 1H), 7.65 (d,1H, J = 7.0 Hz), 7.70 (d, 1H, J = 8.3 Hz), 7.86 (d, 1H, J = 7.8 Hz), 9.49 (d, 1H, J = 7.5 Hz).

To a suspension of intermediate **10** (2.0 g, 3.4 mmol) in THF (131 mL) at room temperature under nitrogen was added solid *N*-bromosuccinimide (630 mg, 3.6 mmol) in one portion. The reaction mixture was stirred at room temperature overnight, at which time the solvent was removed in vacuo leaving a pale-yellow solid. This solid was triturated with cold methanol, collected by filtration, and dried to give 1.98 g (87%) of bromo intermediate **11**. ^{1}H NMR (DMSO-d_6): δ 1.91 (m, 2H), 3.44 (m, 2H), 3.72 (s, 6H), 4.53 (s, 2H), 474 (m, 2H), 4.87 (s, 2H),

6.71 (s, 1H), 6.93 (d, 4H, J = 8.1 Hz), 7.25 (d, 4H, J = 8.1 Hz), 7.37 (m, 2H), 7.59−7.69 (m, 3H), 8.08 (s, 1H), 9.50 (d, 1H, J = 7.0 Hz).

A Schlenk tube was charged with **11** (790 mg, 1.7 mmol), methoxyethanol (25 mL), sodium acetate (570 mg, 7.0 mmol), and dichlorobis(triphenylphosphine)palladium(II) (82 mg, 0.12 mmol). The tube was successively evacuated and filled with carbon monoxide, then heated at 155 °C in an oil bath for 3 h. The reaction mixture was cooled to room temperature, additional CO and $PdCl_2(PPh_3)_2$ were added, and the mixture continued heating for 4 h. The reaction mixture was cooled to room temperature, diluted with methylene chloride, and filtered through Celite. The filtrate was concentrated in vacuo, and the residue was dissolved in ethyl acetate and washed with water. The organic layer was dried over magnesium sulfate, filtered, and concentrated to a solid. The solid was triturated with ethyl ether, collected by filtration, and dried to give 700 mg (85%) of **13** as a light-orange solid. ^{1}H NMR ($CDCl_3$): δ 2.14 (m, 2H), 3.44 (s, 3H), 3.67−3.78 (m, 4H), 3.81 (s, 6H), 4.44 (s, 2H), 4.51 (m, 2H), 4.81 (m, 4H), 6.91 (d, 4H, J = 8.5 Hz), 6.98 (s, 1H), 7.28 (d, 4H, 8.6), 7.34−7.7.61 (m, 4H), 8.21 (d, 1H, J = 8.3 Hz), 8.42 (s, 1H), 9.67 (d, 1H, J = 7.6 Hz).

To a solution of intermediate **13** (960 mg, 1.38 mmol) in CH_2Cl_2 (30 mL) at 0 °C under nitrogen was added thioanisole (3.2 mL, 110 mmol) followed by trifluoroacetic acid (8.5 mL, 27.6 mmol). The mixture was stirred at 0 °C for 1 h, then allowed to warm to room temperature overnight. The solvent was removed under vacuum, leaving a dark-red oil. Ethyl ether was added and a tan solid was collected to give 600 mg (92%) of **14**. ^{1}H NMR (DMSO-d_6): δ 2.29 (m, 2H), 3.3 (m, 2H), 3.73 (m, 2H), 4.45 (m, 2H), 4.54 (m, 3H), 4.82 (m, 2H), 4.99 (s, 2H), 7.40 (m, 2H), 7.58 (d, 1H), 7.85 (d, 1H), 8.13 (d, 1H), 8.52 (s, 1H), 8.6 (s, 1H), 9.49 (d, 1H).

Diol 8 (Method B). To a stirred suspension of **14** (4.4 g, 9.35 mmol) in $CHCl_2$ (220 mL) at 0 °C under nitrogen was added DIBAL-H (10.3 mL of 1 M solution) dropwise. The reaction mixture gradually became homogeneous, and the mixture was stirred at 0 °C for 1 h and then warmed to room temperature for 6 h. The mixture was cooled to 0 °C on an ice bath, and water (50 mL) was slowly added. An aqueous solution of NaOH (1 M, 300 mL) was added, and the reaction mixture was stirred at room temperature for 1 h. The precipitate was collected by filtration to yield 3.6 g (96%) of **8** as a tan solid. This compound was identical in its physical and spectral properties as the material prepared by method A.

Preparation of Tritrifluoroacetate Intermediate 8a. To a suspension of **8** (450 mg, 1.1 mmol) in methylene chloride (30 mL) at 0 °C under nitrogen was added trifluoroacetic anhydride (714 mg, 3.4 mmol) followed by triethylamine (325 mg, 3.4 mmol). The reaction mixture gradually became homogeneous, was stirred at 0 °C for 1 h, and then warmed to room temperature overnight. The mixture was diluted with methylene chloride and washed with water and brine. The organic phase was dried over magnesium sulfate, filtered, and concentrated in vacuo to a solid. This solid was used in the next sequence without further purification.

General Procedure for Ethers and Thioethers 18−31. **8a** was dissolved in the appropriate alcohol (0.025 M) or thiol and heated to 80 °C in an oil bath. The reaction mixture was monitored for disappearance of starting material by HPLC. The mixture was cooled to room temperature and the solvent was removed in vacuo, leaving a solid. The resulting solid was triturated with ether and collected by filtration. The products were further purified using silica gel column chromatography with CH_2Cl_2/MeOH (95:5) as solvent. The HPLC purity of the final products was >96%.

Compound 18. ^{1}H NMR (DMSO-d_6): δ 1.99 (m, 2H), 3.36 (s, 3H), 3.54 (m, 2H), 4.58 (s, 2H), 4.66 (s, 2H), 4.79 (m, 2H), 4.96 (s, 2H), 7.40−7.49 (m, 2H), 7.52 (d, 1H), 7.65−7.84 (m, 2H), 7.98 (s, 1H), 8.60 (s, 1H), 9.51 (d, 1H). MS (m/z): 413 (M + 1), 435 (M + Na). HRMS (FAB) calcd for $C_{26}H_{24}N_2O_3$: 413.1865; found 413.1852.

Compound 19. ^{1}H NMR (DMSO-d_6): δ 1.148 (t, 3H), 1.94 (m, 2H), 3.46−3.52 (m, 4H), 4.53 (s, 2H), 4.60 (s, 2H), 4.73 (m, 2H), 4.91 (s, 2H), 7.36 (m, 3H), 7.48 (d, 1H), 7.64 (m, 2H), 7.90 (s, 1H), 8.55 (s, 1H), 9.47 (d, 1H). MS (m/z): 427 (M + 1). HRMS (FAB) calcd for $C_{27}H_{26}N_2O_3$: 427.2022; found 427.2034.

Compound 20. ^{1}H NMR (DMSO-d_6): δ 0.88 (t, 3H), 1.55 (m, 2H), 1.933 (m, 2H), 3.36−3.58 (m, 4H), 4.53 (s, 2H), 4.61 (s, 2H), 4.73 (m, 3H), 4.90 (s, 2H), 7.33−7.39 (m 2H), 7.47 (d, 1H), 7.62−7.70 (m, 2H), 8.54 (s, 1H), 9.47 (d, 1H). MS (m/z): 441 (M + 1), 462 (M + Na). HRMS (FAB) calcd for $C_{28}H_{28}N_2O_3$: 441.2178; found 441.2171.

Compound 21. Mp 224−228 °C. ^{1}H NMR (DMSO-d_6): δ 1.15 (d, 6H, 1.92 (m, 2H), 3.45 (m, 2H), 3.67 (m, 1H), 4.52 (s, 2H), 4.61 (s, 2H), 4.73 (m, 2H), 4.89 (s, 2H), 7.3−7.39 (m, 2H0, 7.47 (d, 1H), 7.62−7.69 (m, 2H), 7.89 (s, 1H), 8.54 (s, 1H), 9.47 (d, 1H). MS (m/z): 441 (M + 1). HRMS (FAB) calcd for $C_{28}H_{28}N_2O_3$: 441.2178; found 441.2183.

Compound (±)-22. ^{1}H NMR ($CDCl_3$): δ 0.98 (t, 3H), 1.26 (d, 3H), 1.65 (m, 2H), 2.03 (m, 2H), 3.56 (m, 2H), 4.095 (m, 1H), 4.24 (s, 2H), 4.57 (m 2H), 4.70 (m, 2H), 4.71 (s, 2H), 6.12 (s, 1H), 7.33 (t, 1H), 7.42−7.58 (m, 4H), 7.75 (s, 1H), 9.48 (d, 1H). MS (m/z): 455 (M + 1). HRMS (FAB) calcd for $C_{29}H_{30}N_2O_3$: 455.2335; found 455.2342.

Compound (*S*)-23. ^{1}H NMR ($CDCl_3$): δ 0.98 (t, 3H), 1.26 (d, 3H), 1.65 (m, 2H), 2.03 (m, 2H), 3.56 (m, 2H), 4.095 (m, 1H), 4.24 (s, 2H), 4.57 (m 2H), 4.70 (m, 3H), 4.71 (s, 2H), 6.12 (s, 1H), 7.33 (t, 1H), 7.42−7.58 (m, 4H), 7.75 (s, 1H), 9.48 (d, 1H). MS (m/z): 455 (M + 1). HRMS (FAB) calcd for $C_{29}H_{30}N_2O_3$: 455.2335; found 455.2322.

Compound (*R*)-24. ^{1}H NMR ($CDCl_3$): δ 0.98(t, 3H), 1.26 (d, 3H), 1.65 (m, 2H), 2.03 (m, 2H), 3.56 (m, 2H), 4.095 (m, 1H), 4.24 (s, 2H), 4.57 (m 2H), 4.70 (m, 2H), 4.71 (s, 2H), 6.12 (s, 1H), 7.33 (t, 1H), 7.42−7.58 (m, 4H), 7.75 (s, 1H), 9.48 (d, 1H). MS (m/z): 455 (M + 1). HRMS (FAB) calcd for $C_{29}H_{30}N_2O_3$: 455.2335; found 455.2339.

Compound 25. ^{1}H NMR (DMSO-d_6): δ 0.854 (t, 3H), 1.34 (m, 2H), 1.52 (m, 2H), 1.93 (m, 2H), 3.48 (m, 2H), 4.52 (s, 2H), 4.60 (s, 2H), 4.73 (m, 3H), 4.89 (s, 2H), 7.30−7.42 (m, 2H), 7.47 (d, 1H), 7.62−7.70 (m, 2H), 7.89 (s, 1H), 8.54 (s, 1H), 9.47 (d, 1H). MS (m/z): 455 (M + 1). HRMS (FAB) calcd for $C_{29}H_{30}N_2O_3$: 455.2335; found 455.2337.

Compound 26. ^{1}H NMR (DMSO-d_6): δ 1.28 (s, 9H), 1.97 (m, 2H), 3.62 (m, 2H), 4.56 (s, 2H), 4.52 (s, 2H), 4.77 (m, 3H), 4.94 (s, 2H), 7.35−7.72 (3m, 3H), 7.72 (m, 2H), 7.90 (s, 1H), 8.8.57 (s, 1H), 9.50 (d, 1H). MS (m/z): 455 (M + 1), 477 (M + Na). HRMS (FAB) calcd for $C_{29}H_{30}N_2O_3$: 455.2335; found 455.2350.

Compound 27. ^{1}H NMR (DMSO-d_6): δ 0.87 (t, 6H), 1.50 (m, 4H), 1.93 (m, 2H), 3.46 (m, 2H), 4.52 (s, 2H), 4.62 (s, 2H), 4.73 (m, 3H), 4.89 (s, 2H), 7.37 (m, 2H), 7.48 (m, 1H), 7.66 (m, 2H), 7.91 (s, 1H), 8.54 (s, 1H), 9.47 (d, 1H). MS (m/z): 469 (M + 1). HRMS (FAB) calcd for $C_{30}H_{32}N_2O_3$: 469.2491; found 469.2496.

Compound 28. ^{1}H NMR (DMSO-d_6): δ 0.89 (d, 6H), 1.47 (m, 2H), 1.70 (m, 1H), 1.96 (m, 2H), 3.52 (m, 4H), 4.56 (s, 2H), 4.64 (s, 2H), 4.77 (m, 2H), 4.93 (s, 2H), 7.40 (m, 2H), 7.51 (d, 1H), 7.69 (m, 2H), 7.94 (s, 1H), 8.58 (s, 1H), 9.48 (d, 1H). MS (m/z): 469 (M + Na). HRMS (FAB) calcd for $C_{30}H_{32}N_2O_3$: 469.2491; found 469.2491.

Compound 29. ^{1}H NMR (DMSO-d_6): δ 1.17 (t, 3H), 1.93 (m, 2H), 2.42 (q, 2H), 3.48 (m, 2H), 3.93 (s, 2H), 4.52 (s, 2H), 4.72 (m, 3H), 4.89 (s, 2H), 7.33−7.49 (m, 3H), 7.65 (m, 2H), 7.88 (s, 1H), 8.56 (s, 1H), 9.46 (d, 1H). MS (m/z): 443 (M + 1). HRMS (FAB) calcd for $C_{27}H_{26}N_2O_2S$: 443.1793; found 443.2174.

Compound 30. ^{1}H NMR ($CDCl_3$): δ 1.31 (d, 6H), 2.34 (m, 2H), 2.86 (m, 1H), 3.98 (s, 2H), 4.29 (s, 2H), 4.45 (m, 1H), 4.74 (m, 2H), 4.92 (s, 2H), 6.07 (s, 1H), 7.39 (m, 2H), 7.51 (m, 2H), 7.57 (m, 1H), 7.80 (s, 1H), 9.53 (d, 1H). MS (m/z): 457 (M + 1), 479 (M + Na). HRMS (FAB) calcd for $C_{28}H_{28}N_2O_2S$: 457.1950; found 457.1945.

Compound 31. This compound was isolated by chromatography from the reaction of **30**. ^{1}H NMR (DMSO-d_6): δ 1.21 (dd, 6H), 1.93 (m, 2H), 2.82 (m, 1H), 3.49 (m, 2H), 4.12 (d, 1H), 4.23 (d, 1H), 2.52 (s, 2H), 4.75 (m, 3H), 4.88 (s, 2H), 7.33−7.45 (m, 2H), 7.55 (d, 1H), 7.65 (d, 1H), 7.71 (d, 1H), 7.94 (s,

1H), 8.58 (s, 1H), 9.47 (d, 1H). MS (*m*/*z*): 494 (M + Na). HRMS (FAB) calcd for $C_{28}H_{28}N_2O_3S$: 473.1899; found 473.1886.

9-(1-Oxoethyl)-12-(3-aceoxypropyl)-6*H*,7*H*,13*H*-indeno[2,1-*a*]pyrrolo[3,4-*c*]carbazole-5-one (15). To a suspension of aluminum chloride (335 mg, 2.2 mmol) in 1,2-dichloroethane/methylene chloride (1:1, 8 mL) was added acetyl chloride (172 mg, 2.2 mmol) under nitrogen. The reaction mixture was cooled to 0 °C in an ice bath, and a suspension of **5** (310 mg, 0.84 mmol) in methylene chloride (3 mL) was added dropwise. The ice bath was removed, and the reaction mixture was warmed to room temperature and heated to reflux for 2 h. The mixture was cooled to room temperature and poured over ice/water, and concentrated HCl (5 mL) was added. The precipitate was collected by filtration and dried to give 340 mg (89%) of **15**. ^{1}H NMR (DMSO-d_6): δ 2.02 (s, 3H), 2.18 (m, 2H), 2.74 (s, 3H), 4.12 (m, 2H), 4.56 (s, 2H), 4.83 (m, 2H), 5.05 (s, 2H), 7.43 (m, 2H), 7.68 (d, 1H), 7.86 (d, 1H), 8.17 (d, 1H), 8.56 (s, 1H), 8.72 (1H), 9.53 (d, 1H). MS (*m*/*z*): 453 (M + 1).

9-(1-Hydroxyethyl)-12-(3-hydroxypropyl)-6*H*,7*H*,13*H*-indeno[2,1-*a*]pyrrolo[3,4-*c*]carbazole-5-one (16). To a suspension of **15** (82 mg, 0.18 mmol) in THF (6 mL) under nitrogen was added lithium borohydride (0.9 mL of 2 M solution in THF) at 0 °C. The reaction mixture was stirred at 0 °C for 1 h, then warmed to room temperature for 4 h. The mixture was cooled to 0 °C, methanol was added slowly dropwise, and then the solution was stirred at room temperature overnight. The reaction mixture was diluted with ethyl acetate, washed with water and brine, dried (magnesium sulfate), and concentrated in vacuo to 69 mg (90%) of **16** as a white solid. ^{1}H NMR (DMSO-d_6): δ 1.41 (d, 3H), 1.92 (m, 2H), 3.46 (m, 2H), 4.52 (s, 2H), 4.71 (m, 3H), 4.89 (s, 3H), 5.18 (s, 1H), 7.32−7.39 (m, 2H), 7.50 (d, 1H), 7.64 (m, 2H), 7.89 (s, 1H), 8.55 (s, 1H), 9.46 (d, 1H). MS (*m*/*z*): 413 (M + 1), 435 (M + Na).

9-(1-Oxoethyl)-12-(3-hydroxypropyl)-6*H*,7*H*,13*H*-indeno[2,1-*a*]pyrrolo[3,4-*c*]carbazole-5-one (17). To a stirred solution of **15** (55 mg, 0.122 mmol) in methanol/THF (8 mL, 3:1) at room temperature was added potassium carbonate (16.8 mg, 0.122 mmol), and the mixture was heated to reflux for 30 min. The reaction mixture was cooled to room temperature overnight and the solvent was removed in vacuo, giving a white solid. The solid was triturated with water and collected by filtration. The solid was purified by flash chromatography on silica gel using ethyl acetate (100%), then methanol/ethyl acetate (10%) to give 38 mg (76%, 96% purity by HPLC) of **17**. ^{1}H NMR (DMSO-d_6): δ 1.95 (m, 2H), 2.69 (s, 3H), 3.47 (m, 2H), 4.54 (s, 2H), 4.77 (m, 2H), 5.00 (s, 2H), 7.37 (m, 2H), 7.64 (m, 1H), 7.82 (d, 1H), 8.11 (d, 1H), 8.51 (s, 1H), 8.66 (s, 1H), 9.48 (d, 1H). MS (*m*/*z*): 411 (M + 1).

Compounds **32**−**37** were prepared by the method described for **18**−**31** using **16** according to the general procedure for tritrifluoroacetate intermediate **8a**. The products were further purified using silica gel column chromatography with CH_2Cl_2/MeOH (95:5) as solvent. The HPLC purity of the final products was >96%.

Compound (±)-32. ^{1}H NMR (DMSO-d_6): δ 1.08 (t, 3H), 1.41 (d, 3H), 1.93 (m, 2H), 3.47 (m, 2H), 4.52 (s, 2H), 4.60 (m, 1H), 4.73 (m, 2H), 4.90 (m, 2H), 7.33−7.39 (m, 2H), 7.47 (d, 1H), 7.63 (d, 1H), 7.69 (d, 1H), 7.86 (s, 1H), 8.55 (s, 1H), 9.47 (d, 1H). MS (*m*/*z*): 441 (M + 1), 395 (M − OCH_2CH_3). HRMS (FAB) calcd for $C_{28}H_{28}N_2O_3$: 441.2178; found 441.2159.

Chiral HPLC Separation of (±)-32. Racemic **32** (15 mg) was separated on a Chiralcel OD column (1 cm × 25 cm) using hexanes/ethanol (1:4, flow rate 0.5 mL/min) solvent system to give enantiomer **33** (3.6 mg) and **34** (2.8 mg). Compound **33** (chiral): t_R = 27.9 min. MS (*m*/*z*): 441 (M + 1), 395 (M − OCH_2CH_3). Compound **34** (chiral): t_R = 50.9 min. MS (*m*/*z*) 441 (M + 1), 395 (M − OCH_2CH_3). Because of the low recovery under the conditions to achieve separation of the enantiomers, only milligram quantities could be obtained for kinase screening.

Compound (±)-35. ^{1}H NMR (DMSO-d_6): δ 1.45 (d, 3H), 1.98 (m, 2H), 3.14 (s, 3H), 3.50 (m, 2H), 4.58 (m, 3H), 7.75 (m, 2H), 4.93 (s, 2H), 7.33 (m, 2H), 7.48 (d, 1H), 7.67 (d, 1H), 7.72 (d, 1H), 7.88 (s, 1H), 8.58 (s, 1H), 9.49 (d, 1H). MS (*m*/*z*): 427 (M + 1). HRMS (FAB) calcd for $C_{27}H_{26}N_2O_3$: 427.2022; found 427.2035.

Compound (±)-36. ^{1}H NMR (DMSO-d_6): δ 1.01 (d, 3H), 1.10 (d, 3H), 1.38 (d, 3H), 1.95 (m, 2H), 3.47 (m, 2H), 3.98 (q, 1H), 4.26 (m, 1H), 4.52 (s, 2H), 4.74 (m, 3H), 4.90 (m, 2H), 7.33−7.39 (m, 2H), 7.48 (d, 1H), 7.62−7.69 (m, 2H), 7.87 (s, 1H), 8.54 (s, 1H), 9.47 (d, 1H). MS (*m*/*z*): 455 (M + 1). HRMS (FAB) calcd for $C_{29}H_{30}N_2O_3$: 455.2335; found 455.2321.

Compound (±)-37. ^{1}H NMR (DMSO-d_6): δ 0.81 (t, 3H), 1.27−1.43 (m, 7H), 1.93 (m, 2H), 3.48 (m, 2H), 4.53 (s, 2H), 4.58 (m, 1H), 4.73 (m, 4H), 4.92 (m, 2H), 7.33−7.39 (m, 2H), 7.46 (d, 1H), 7.63 (d, 1H), 7.69 (d, 1H), 7.86 (s, 1H), 8.55 (s, 1H), 9.47 (d, 1H). MS (*m*/*z*): 469 (M + 1). HRMS (FAB) calcd for $C_{30}H_{32}N_2O_3$: 469.2491; found 469.2503.

9-(Isopropoxymethyl)-6*H*,7*H*,12*H*,13*H*-indeno[2,1-*a*]-pyrrolo[3,4-*c*]carbazole-5-one (38). This compound was prepared from 9-(hydroxymethyl)indeno[2,1-*a*]pyrrolo[3,4-*c*]-carbazole-5-one according to the general procedure for ether formation for tritrifluoroacetate intermediate **8a**. Precipitation from DMF/ether gave **38** as a white solid (85%, 97% purity). ^{1}H NMR (DMSO-d_6): δ 1.15 (d, 6H), 3.68 (m, 1H), 4.13 (s, 2H), 4.59 (s, 2H), 4.89 (s, 2H), 7.28−7.42 (m, 3H), 7.54 (d, 1H), 7.64 (d, 1H), 7.88 (s, 1H), 8.49 (s, 1H), 9.35 (d, 1H), 11.87 (s, 1H). MS (*m*/*z*): 383 (M + 1). HRMS (FAB) calcd for $C_{25}H_{22}N_2O_2$: 383.1759; found 383.1754.

9-(Carboxaldehyde)-12-(3-hydroxypropyl)-6*H*,7*H*,13*H*-indeno[2,1-*a*]pyrrolo[3,4-*c*]carbazole-5-one (39). Step 1. To a well-stirred suspension of **5** (4.4 g, 11.9 mmol) in a mixture of 1-methyl-2-pyrrolidinone (51 mL) and methylene chloride (51 mL) were added sequentially triethylamine (2.99 g, 29.6 mmol), a catalytic amount of 4-(dimethylamino)pyridine (0.2 g), and acetic anhydride (3.04 g, 29.8 mmol) at room temperature. After 16 h at room temperature, the reaction was quenched with water (150 mL) and methylene chloride was removed under vacuum. The solid was filtered, washed with water, and dried to give 4.5 g (90%) of the *O*-acetate intermediate **39a**. ^{1}H NMR (DMSO-d_6): δ 2.01 (s, 3H), 2.06−2.18 (m, 2H), 4.06−4.16 (m, 2H), 4.51 (s, 2H), 4.75−4.87 (m, 2H), 4.92 (s, 2H), 7.27−7.78 (m, 6H), 8.00 (d, 1H), 8.54 (s, 1H), 9.51 (d, 2H).

Step 2. To a well-stirred suspension of **39a** (0.5 g, 1.21 mmol) and 1,1-dichloromethyl methyl ether (1.39 g, 12.19 mmol) in a mixture of methylene chloride (42 mL) and toluene (5 mL) was added tin(IV) chloride (2.37 g, 9.11 mmol) (1 M solution in methylene chloride) at room temperature. The reaction mixture was further stirred at room temperature for 4 h and at 50 °C for 45 min, then quenched with aqueous 2 N HCl (25 mL) at room temperature. Methylene chloride was removed under vacuum, and the aqueous layer was triturated with *tert*-butylmethyl methyl ether (30 mL) at room temperature for 14 h. The solid was filtered, washed with water and *tert*-butylmethyl methyl ether, and then dried to obtain a crude product, which was triturated with *tert*-butylmethyl methyl ether (20 mL), to give 430 mg (81%) of aldehyde **39b**. ^{1}H NMR (DMSO-d_6): δ 2.00 (s, 3H), 2.15−2.27 (m, 2H), 4.10−4.16 (m, 2H), 4.48 (s, 2H), 4.76−4.90 (m, 2H), 4.95 (s, 2H), 7.33−7.45 (m, 2H), 7.64 (d, 1H), 7.89 (d, 1H), 8.04 (d, 1H), 8.51 (s, 1H), 8.64 (s, 1H), 9.51 (d, 1H), 10.11 (s, 1H). MS *m*/*z* 439 (M + 1).

Step 3. To a well-stirred solution of **39b** (0.021 g, 0.048 mmol) in 1-methyl-2-pyrrolidinone (2 mL) was added sodium methoxide in methanol (2 mL, 2 M solution) at room temperature, and the resulting mixture was stirred at room temperature for 45 min, then quenched with water (50 mL). The solid was filtered, washed with water, and dried to give 17 mg (93%) of **39** as an orange solid. ^{1}H NMR (DMSO-d_6): δ 1.98−2.00 (m, 2H), 3.50−3.54 (m, 2H), 4.54 (s, 2H), 4.77−4.81 (m, 2H), 4.98 (s, 2H), 7.36−7.45 (m, 2H), 7.665 (d, 1H), 7.90 (d, 1H), 8.04 (d, 1H), 8.53 (s, 1H), 8.64 (s, 1H), 9.51 (d, 1H), 10.11 (s, 1H). MS (*m*/*z*): 397 (M + 1).

Dimethylglycine Ester 40. An oven-dried, 3 L three-necked, round-bottomed flask equipped with a mechanical stirrer, a three-way stopcock connected to an argon balloon, and an immersion thermometer was charged with **21** (65.4 g,

148.6 mmol) followed by anhydrous *N*,*N*-dimethylacetamide (654 mL). 4-(Dimethylamino)pyridine (9 g, 73.7 mmol), *N*,*N*-dimethylglycine (38.2 g, 370.8 mmol), and 1-[3-(dimethylamino)propyl]-3-ethylcarbodiimide hydrochloride (70.3 g, 368 mmol) were added sequentially at 35 °C. The suspension was heated to 42−45 °C for 2 h, and additional quantities of 4-(dimethylamino)pyridine (1.5 g, 12.2 mmol), *N*,*N*-dimethylglycine (8 g, 77.6 mmol), and 1-[3-(dimethylamino)propyl]-3-ethylcarbodiimide hydrochloride (15 g, 78.5 mmol) were added sequentially at 42 °C. After 1.5 h, the reaction mixture was cooled to 0−5 °C and the reaction was quenched with water (1310 mL, added dropwise for 35 min). The cooling bath was removed, and the resulting pale-yellow suspension was stirred at room temperature for 1 h. The suspension was filtered, washed with water (2600 mL) to pH 8, and dried overnight. The solid was dissolved in CH_2Cl_2 (800 mL) and washed with water and brine (2 × 200 mL), dried ($MgSO_4$), filtered, and concentrated. The crude material was dissolved in CH_2Cl_2 (217 mL) and transferred into a 3 L three-necked round-bottomed flask, which was equipped with a mechanical stirrer. Ethyl acetate (1000 mL) was added dropwise at room temperature to the clear-red solution for 1 h and 10 min, and then the mixture was stirred for 2.5 h at room temperature and filtered. The solid was washed sequentially with ethyl acetate (80 mL), ethyl acetate (75 mL)/methyl *tert*-butyl ether (50 mL), and methyl *tert*-butyl ether (2 × 60 mL) and dried to obtain 62 g (97.8% purity, 78% yield) of **40** as an off-white solid, mp 193−94 °C. ^{1}H NMR (DMSO-d_6): δ 1.195 (d, 6H), 2.13−2.18 (m, 2H), 2.21 (s, 6H), 3.10 (s, 2H), 3.70−3.76 (m, 2H), 4.10−4.13 (m, 2H), 4.46 (s, 2H), 4.64 (s, 2H), 4.71−4.75 (m, 2H), 4.87 (s, 2H), 7.35−7.69 ((m, 4H), 7.89 (s, 1H), 8.53 (s, 1H), 9.50 (d, 1H). MS (*m*/*z*): 527 (M + 1).

9-(Methyl)-12-(3-hydroxypropyl)-6*H*,7*H*,13*H*-indeno-[2,1-*a*]pyrrolo[3,4-*c*]carbazole-5-one (41). To a stirred suspension of **8** (60 mg, 0.151 mmol) in methylene chloride (6 mL) at 0 °C under nitrogen was added trifluoroacetic anhydride (11.4 μL, 0.181 mmol) followed by triethylsilane (28 μL, 0.181 mmol). The homogeneous mixture was stirred at 0 °C for 1 h, then warmed to room temperature overnight. The reaction solvent was removed in vacuo, leaving a tan solid, which was triturated with ether and collected by filtration. The solid was purified by flash chromatography on silica gel using methanol/chloroform (5%) to give 47 mg (82%) of **41**. ^{1}H NMR (DMSO-d_6): δ 1.91 (m, 2H), 2.46 (s, 3H), 3.45 (m, 2H), 4.51 (s, 2H), 4.70 (m, 2H), 4.89 (s, 2H), 7.35 (m, 3H), 7.61 (m, 2H), 7.77 (s, 1H), 8.53 (s, 1H), 9.46 (d, 1H). MS (*m*/*z*): 383 (M + 1).

VEGF-R2 Receptor-Linked Tyrosine Kinase Assay. Enzyme inhibition studies were performed using a modification of the ELISA described for trkA kinase.[24] Briefly, the 96-well microtiter plate (FluoroNUNC or Costar High Binding) was coated with 10 μg/mL recombinant human PLC-γ/GST. Kinase assays were performed in 100 μL reaction mixtures containing 50 mM HEPES (pH 7.4), K_m level of ATP, 10 mM $MnCl_2$, 0.1% BSA, 2% DMSO, and various concentrations of drug. The reaction was initiated by adding baculoviral recombinant human enzyme VEGF-R2 and allowed to proceed for 15 min at 37 °C. The detection antibody, Eu-N1 antiphosphotyrosine (PT66) antibody, was added. After 1 h of incubation at 37 °C, 100 μL of enhancement solution was added and the plate was gently agitated. After 5 min, the fluorescence of the resulting solution was measured using the Victor^2 multilabel counter.

Recombinant Proteins and Biochemical Kinase Assays. Enzymes and Substrates. The cytoplasmic domains of recombinant human tyrosine kinases (FGF-R1, Flt-3, PDGF-Rβ, Tie2, TrkA, VEGF-R1, VEGF-R2, VEGF-R3) and serine/threonine kinases (CHK1, CDK1/cyclinB, CDS1) were expressed in a baculovirus insect cell system. Recombinant β-insulin receptor kinase (βIrk) was purchased from Stratagene (La Jolla, CA). Purified rat brain protein kinase C (mixture of Ca^{2+}-dependent isozymes α, β, and γ) and activated recombinant human GST-p38α were obtained from Upstate Biotechnology, Inc. (Lake Placid, NY). Phospholipase C-γ was generated as a fusion protein with glutathione S-transferase following the procedure of Rotin et al.[33] Histone H-1 and MBP were purchased from Fluka Chemical Corp. (Milwaukee, WI) and Upstate Biotechnology, Inc. (Lake Placid, NY), respectively. Time-resolved fluorescence experiments were performed using Eu-N1 antiphosphotyrosine antibody, Eu-N1 antiphosphothreonine antibody, Eu-N1 antirabbit IgG, and DELFIA enhancement solution purchased from Perkin-Elmer Life Sciences (Gaithersburg, MD).

Receptor-Linked Tyrosine Kinase Assays. Enzyme inhibition studies were performed as described for VEGFR-2, using a modification of the ELISA described for trkA kinase at the K_m level of ATP.[24] Inhibition curves were generated by plotting percent control activity versus log of the concentration of compound. IC_{50} values were calculated by nonlinear regression using the sigmoidal dose−response (variable slope) equation in GraphPad Prism. IC_{50} values were reported as the average of at least three separate determinations.

Human Endothelial Cell-Based Receptor Phosphorylation Assay. Subconfluent HUVECs were serum-starved by replacing media with EBM-2 (endothelial cell basal medium, serum-free; Clonetics) containing 0.05% BSA for 1 h at 37 °C, during which time a range of concentrations of drug or DMSO (control) were added to the cells. Human VEGF (Clonetics) was then added to HUVECs at a concentration of 10 ng/mL for 5 min. Cells were lysed in RIPA buffer containing 1 mM activated sodium vanadate and protease inhibitors (Protease Inhibitor Cocktail Set III, Calbiochem), sheared with a 27-gauge syringe, then centrifuged at 12000*g* for 15 min. Clarified cell lysates were normalized to protein using the BCA method (Pierce), immunoprecipitated with anti-VEGF-R2 antibody (CEP-133) for 1 h, followed by incubation with protein A sepharose for another hour at 4 °C. Immunoprecipitates were washed three times with RIPA buffer, 4X sample buffer was added, and the mixture was heated for 5 min at 85 °C. Samples were separated on a 6% Tris-glycine gel (NOVEX) or NuPAGE 7% Tris-acetate gel (NOVEX) and transferred using a wet blot system onto a Millipore PVDF membrane. The membrane was blocked with SuperBlock buffer (Pierce) containing 0.05% Tween-20, immunoblotted with 4G10 antiphosphotyrosine antibody (UBI; diluted 1:1000 in TBS-T containing 3% BSA) for 1−2 h, followed by incubation with horseradish peroxidase coupled goat antimouse IgG (BioRad; diluted 1:20000 in TBS-T containing 3% BSA) for 1 h. Phosphorylated proteins were visualized using enhanced chemiluminescence (Amersham). The percent inhibition was calculated by analyzing scanned autoradiographs on a densitometer. Scores were based on a decrease in protein band density compared to that of VEGF-stimulated control (no inhibitor) as follows: 0 = no decrease; 1 = 1−25%; 2 = 26−50%; 3 = 51−75%; 4 = 76−100%.

In Vitro Capillary Tube Formation Assay with HUVECs on Matrigel and ex Vivo Rat Aortic Ring Explant Assay in Collagen Gel Matrixes. The ability of **21** to inhibit angiogenesis in vitro in a capillary tube formation assay utilizing HUVECs cultured on a synthetic basement membrane matrix and ex vivo in rat aortic ring explant cultures was conducted using published methods.[30]

Pharmacokinetics in Rat. Single-dose oral administration of test compounds in fasted adult male Sprague−Dawley rat (n = 3) was delivered via oral gavage in a dose volume of 2 mL/kg. Compound **21** was delivered in a 3:1 geluceire/PG vehicle. Compound **40** was delivered in distilled water or 1% HOAc. A dose of 1.19 mg/kg **40** is equivalent to a 1.0 mg/kg dose of **21**. The blood samples were placed on wet ice, and plasma was collected after centrifugation. Plasma samples were frozen on dry ice and stored frozen at −20 °C prior to analysis. Plasma was prepared for high-performance liquid chromatography (HPLC)/mass spectrometric analysis by protein precipitation with two volumes of acetonitrile (200 μL) per 100 μL sample of plasma. The plasma samples were then analyzed for both CEP-7055 and CEP-5214 via HPLC coupled with tandem mass spectrometry. The data were entered into an Excel spreadsheet, and pharmacokinetic parameters were determined by WinNonLin.

In Vivo Antitumor Activity in the Subcutaneous SVR Angiosarcoma Xenograft Model in Nude Mice. The oral efficacy of **21** and **40** was evaluated on the growth of SVR angiosarcoma xenografts in nude mice.[32] Female athymic nu/nu mice (6−8 weeks old) were maintained five per cage in microisolator units on a standard sterilizable laboratory diet (Teklad Labchow). Mice were quarantined 1 week prior to experimental manipulation. Tumor growth was initiated following the sc implantation of subconfluent cultures into the right flank of female athymic nude mice in their respective serum-free media along with Matrigel (Collaborative Research) synthetic basement membrane (1:1 v/v). The SVR murine angiosarcoma cell line at 1×10^6 cell density was implanted in vivo. When tumors achieved volumes of 80−180 mm^3, tumor-bearing nude mice for each xenograft were randomized into treatment groups (usually 8−10 mice/group) and oral b.i.d. ($T = 0$, 8 h) administration of **21** (PG: Tween 80; 1:1) or **40** (1% HOAc solution) was initiated at doses ranging from 0.35 to 23.8 mg/kg in a vehicle at 100 μL/dose. Tumor volumes were determined with vernier calipers every 3−4 days by measuring the largest perpendicular diameters using the formula

$$V\ (\mathrm{mm}^3) = (0.5236)[\text{length (mm)}][\text{width (mm)}]\left[\frac{\text{length (mm)} + \text{width (mm)}}{2}\right]$$

Tumor measurements were expressed as absolute volumes, as well as normalized to individual tumor volumes at day 1, the initiation of dosing (relative tumor volumes) to assess changes in the rate of tumor growth relative to treatment. Statistical analyses of tumor data were done using the Mann−Whitney rank sum test or, when appropriate for the data set, by one-way ANOVA and the Dunnet's multiple comparison test, with $p < 0.05$ being deemed significant. Animal body weights were determined and analyzed over a similar time course.

Acknowledgment. The authors gratefully acknowledge the scientific support and consultation of Stuart Dodson, Mary Ann Harris, Joe Herman, Beverly Holskin, Jean Husten, Nelson Landmesser, Chung Ho Park, Alyssa Reiboldt, Damaris Rolon-Steele, and Santhe Spais.

References

(1) Folkman, J. Angiogenesis-dependent diseases. *Semin. Oncol.* **2001**, *28*, 536−542.
(2) Carmeliet, P.; Jain, R. K. Angiogenesis in cancer and other diseases. *Nature* **2000**, *407*, 249−257.
(3) Griffioen, A. W.; Molema, G. Angiogenesis: potentials for pharmacologic intervention in the treatment of cancer, cardiovascular diseases, and chronic inflammation. *Pharmacol. Rev.* **2000**, *52*, 237−268.
(4) Folkman, J. Angiogenesis in cancer, vascular, rheumatoid and other disease. *Nat. Med.* **1995**, *1*, 27−31.
(5) Fan, T. P. D.; Jaggar, R.; Bicknell, R. Controlling the vasculature: angiogenesis, anti-angiogenesis, and vascular targeting of gene therapy. *Trends Pharmacol. Sci.* **1995**, *16*, 57−66.
(6) Gimbrone, M. Receptor tyrosine kinase as targets for inhibition of angiogenesis. *Drug Discovery Today* **1997**, *2*, 50−63.
(7) (a) Thomas, K. A. Vascular endothelial growth factor, a potent and selective angiogenic agent. *J. Biol. Chem.* **1996**, *271*, 603−606. (b) Ferrara, N.; Davis-Smyth, T. The biology of vascular endothelial growth factor. *Endocr. Rev.* **1997**, *18*, 4−25. (c) Klagsburn, M.; Moses, M. A. Molecular angiogenesis. *Chem. Biol.* **1999**, *6*, R217−R227.
(8) (a) Salvern, P.; Heikkila, P.; Joensuu, H. Enhanced expression of vascular endothelial growth factor in metastatic melanoma. *Br. J. Cancer* **1997**, *76*, 930−934. (b) Shibusa, T.; Shijubo, N.; Abe, S. Tumour angiogenesis and vascular endothelial growth factor expression in stage I lung adrenocarcinoma. *Clin. Cancer Res.* **1944**, *4*, 1483−1487. (c) Okita, S.; Kondoh, S.; Shiraishi, K.; Kaino, S.; Hatano, S.; Okita, K. Expression of vascular endothelial growth factor correlates with tumour progression in gallbladder cancer clinical studies. *Int. J. Oncol.* **1998**, *12*, 1013−1018. (d) Abdulrauf, S. I. Edvardsen, K.; Ho, K. L.; Yang, X. Y.; Rock, J. P.; Rosenblum, M. L. Vascular endothelial growth factor expression and vascular density as prognostic markers of survival in patients with low grade astrocytoma. *J. Neurosurg.* **1998**, *88*, 513−520.
(9) Neufeld, G.; Cohen, T.; Gengrinovitch, S.; Poltorak, Z. Vascular endothelial growth factor (VEGF) and its receptors. *FASEB J.* **1999**, *13*, 9−22.
(10) Rahim, N.; Dayanir, V.; Lashkari, K. Receptor chimeras indicate that the vascular endothelial growth factor receptor-1 modulates mitogenic activity of VEGF-R2 in endothelial cells. *J. Biol. Chem.* **2000**, *275*, 16986−16992.
(11) Gille, H.; Kowalski, J.; Li, B.; LeCouter, J.; Moffat, B.; Zioncheck, T. F.; Pelletier, L.; Ferrara, N. Analysis of biological effects and signaling properties of Flt-1 (VEGF-R1) and KDR (VEGF-R2). *J. Biol. Chem.* **2001**, *276*, 3222−3230.
(12) (a) Korpelainen, E. I.; Alitalo, K. Signaling angiogenesis and lymphangiogenesis. *Curr. Opin. Cell Biol.* **1998**, *10*, 159−164. (b) Kukk, E.; Lymboussaki, A.; Taira, S.; Kaipainen, A.; Jeltsch, M.; Joukov, V.; Alitalo, K. VEGF-C receptor binding and pattern of expression with VEGF-R3 suggests a role in lymphatic vascular development. *Development* **1996**, *122*, 3829−3837.
(13) Folkman, J. In *Cancer Medicine*, 5th ed.; Holland, J. E., Frei, I. E., Bast, J., Kufe, D., Pollock, R., Weichselbaum, R., Eds.; B. C. Dekker, Inc.: Ontario, Canada, 2000; pp 132−152.
(14) (a) Deplanque, G.; Harris, A. L. Anti-angiogenic agents: clinical trial design and therapies in development. *Eur. J. Cancer* **2000**, *36*, 1713−1724. (b) Cristofanilli, M.; Charnsangavej, C.; Hortobagyi, G. N. Angiogenesis Modulation in Cancer Research: Novel Clinical Approaches. *Nat. Rev. Drug Discovery* **2002**, *1*, 415−426. (c) Sepp-Lorenzino, L.; Thomas, K. A. *Expert Opin. Invest. Drugs* **2002**, *11*, 1−18.
(15) Sun, L.; McMahon, G. Inhibition of tumor angiogenesis by synthetic receptor tyrosine kinase inhibitors. *Drug Discovery Today* **2000**, *5*, 344−354.
(16) (a) Drevs, J.; Muller-Driver, R.; Wittig, C.; Fuxius, S.; Esser, N.; Hugenschmidt, H.; Konerding, M. A.; Allegrini, P. R.; Wood, J.; Hennig, J.; Unger, C.; Marme, D. PTK787/ZK222584, a specific vascular endothelial growth factor-receptor tyrosine kinase inhibitor, effects the anatomy of the tumor vascular bed and the functional vascular properties as detected by dynamic enhanced magnetic resonance imaging. *Cancer Res.* **2002**, *62*, 4015−4022. (b) Baker, C. H.; Solorzano, C. C.; Fidler, I. J. Blockade of vascular endothelial growth factor receptor and epidermal growth factor receptor signaling for therapy of metastatic human pancreatic cancer. *Cancer Res.* **2002**, *62*, 1996−2003. (c) Bold, G.; Altman, K.-H.; Frei, J.; Lang, M.; Manley, P. W.; Traxler, P.; Weitfeld, B.; Bruggen, J.; Buschdunger, E.; Cozens, R.; Ferrari, S.; Furet, P.; Hofmann, F.; Martiny-Baron, G.; Mestan, J.; Rosel, J.; Sills, M.; Stover, D.; Acemoglu, F.; Boss, E.; Emmenegger, R.; Lasser, L.; Masso, E.; Roth, R.; Schlachter, C.; Vetterli, W.; Wyxx, D.; Wood, J. M. New anilinophthalazines as potent and orally well absorbed inhibitors of the VEGF receptor tyrosine kinase useful as antagonists of tumor-driven angiogenesis. *J. Med. Chem.* **2000**, *43*, 2310−2323.
(17) (a) Hennequin, L. F.; Stokes, E. S.; Thomas, A, P.; Johnstone, C.; Ple, P. A.; Ogilvie, D. J.; Dukes, M.; Wedge, S. R.; Kendrew, J.; Curwen, J. O. Novel 4-anilinoquinazolines with C-7 basic side chains: design and structure activity relationship of a series of potent, orally active, VEGF receptor tyrosine kinase inhibitors. *J. Med. Chem.* **2002**, *45*, 1300−1312. (b) Wedge, S. R.; Ogilvie, D. J.; Dukes, M.; Kendrew, J.; Chester, R.; Jackson, J. A.; Boffey, S. J.; Valentine, P. J.; Curwen, J. O.; Musgrove, H. L.; Graham, G. A.; Hughes, G. D.; Thomas, A. P.; Stokes, E. S. E.; Curry, B.; Richmond, G. H. P.; Wadsworth, P. F.; Bigley, A. L.; Hennequin, L. F. ZD6474 inhibits vascular endothelial growth factor signaling, angiogenesis, and tumor growth following oral administration. *Cancer Res.* **2002**, *62*, 4645−4655.
(18) Jani, J. P.; Beebe, J. S.; Emerson, E.; Gant, T.; Goodwin, P.; Higdon, C.; Hillerman, S.; Intrieri, C.; Knauth, L.; Marx, M.; Noe, M.; Rossi, A. M.; Savage, D.; Atherton, J.; Floyd, E.; Harriman, S.; Roberts, G. CP-547,632, a novel VEGF-R2 tyrosine kinase inhibitor for cancer therapy. *Proc. Am. Assoc. Cancer Res.* **2002**, *43*, 5354.
(19) (a) Gingrich, D. E.; Hudkins, R. L. Selected fused pyrrolocarbazoles. Patent WO 0217914, 2002. (b) Pili, R.; Robinson, C.; Morris, C. A.; Dionne, C. A.; Isaacs, J. T.; Ruggeri, B. A. CEP-5214, a novel orally-active inhibitor of vascular endothelial growth factor (VEGF) receptor tyrosine kinases, inhibits VEGF-induced angiogenesis and prostate tumor growth in vivo. *Clin. Cancer Res.* **2001**, *7*, 3658s.
(20) Hudkins, R. L.; Knight, E., Jr. Fused pyrrolocarbazole. U.S. Patent 5,705,511, 1997.
(21) Hudkins, R. L.; Park, C.-H. Synthesis of indeno[2,1-*a*]pyrrolo-[3,4-*c*]carbazole lactam regioisomers using ethyl *cis*-β-cyanoacrylate as a dienophile and lactam precursor. *J. Heterocycl. Chem.* **2003**, *40*, 135−142.
(22) Kaneko, M.; Saito, Y.; Saito, H.; Matsumoto, T.; Matsuda, Y.; Vaught, J. L.; Dionne, C. A.; Angeles, T. S.; Glicksman, M. A.; Neff, N. T.; Rotella, D. P.; Kauer, J. C.; Mallamo, J. P.; Hudkins, R. L.; Murakata, C. Neurotrophic 3,9-bis[(alkylthiomethyl]- and -[bis(alkoxymethyl)]-K-252a derivatives. *J. Med. Chem.* **1997**, *40*, 1863−1869.

(23) Synthesis of esters. In *Carbonylation: Direct Synthesis of Carbonyl Compounds*; Colquhoun, H. M., Thompson, D. J., Twigg, M. V., Eds.; Plenum Press: New York, 1991; pp 111−141.
(24) Angles, T. S.; Steffler, C.; Bartlett, B. A.; Hudkins, R. L.; Stephens, R. M.; Kaplan, D. R.; Dionne, C. A. Enzyme linked immunosorbant assay for TrkA tyrosine kinase activity. *Anal. Biochem*. **1996**, *236*, 49−55.
(25) Mohammadi, M.; McMahon, G.; Sun, L.; Tang, C.; Hirth, P.; Yeh, B. K.; Hubbard, S. R.; Schlessinger, J. Structures of the tyrosine kinase domain of fibroblast growth factor receptor in complex with inhibitors. *Science* **1997**, *276*, 955−960.
(26) Mctigue, M. A.; Wickersham, J. A.; Pinko, C.; Showalter, R. E.; Parast, C. V.; Tempczyk-Russell, A.; Gehring, M. R.; Mroczkowski, B.; Kan, C. C.; Villafranca, J. E.; Appelt, K. Crystal Structure of the Kinase Domain of Human Vascular Endothelial Growth Factor Receptor 2: A Key Enzyme in Angiogenesis. *Structure* **1999**, *7*, 319−330.
(27) Toledo, L. M.; Lydon, N. B. Structures of staurosporine bound to CDK2 and cPKA−new tools for structure-based design of protein kinase inhibitors. *Curr. Biol*. **1997**, *5*, 1551−1556.
(28) Hudkins, R. L.; Iqbal, M.; Park, C.-H.; Goldstein, J.; Herman, J. L.; Shek, E.; Murakata, C.; Mallamo, J. P. Prodrug esters of the indolocarbazole CEP-751 (KT-6587). *Bioorg. Med. Chem. Lett*. **1998**, *8*, 1873−1876.
(29) Ruggeri, B.; Singh, J.; Gingrich, D.; Angeles, T.; Albom, M.; Chang, H.; Robinson, C.; Hunter, K.; Dobrzanski, P.; Jones-Bolin, S.; Aimone, L.; Klein-Szanto, A.; Herbert, J.-M.; Bono, F.; Casellas, P.; Bourie, B.; Pili, R.; Isaacs, J.; Ator, M. A.; Hudkins, R.; Dionne, C.; Mallamo, J.; Vaught, J. CEP-7055: A novel, orally-active pan inhibitor of vascular endothelial growth factor receptor tyrosine kinases with potent anti-angiogenic activity and anti-tumor efficacy in pre-clinical models. *Cancer Res*. **2003**, *63*, 5978−91.
(30) (a) Vailhe, B.; Vittet, D.; Feige, J.-J. In vitro models of vasculogenesis and angiogenesis. *Lab. Invest*. **2001**, *81*, 439−452. (b) Ilan, N.; Mahooti, S.; Madri, J. A. Distinct signal transduction pathways are utilized during the tube formation and survival phases of in vitro angiogenesis. *J. Cell Sci*. **1998**, *111*, 3621−3631. (c) Brown, K. J.; Maynes, S. F.; Bezos, A.; Maguire, D. J.; Ford, M. D.; Parish, C. R. A novel in vitro assay for human angiogenesis. *Lab. Invest*. **1996**, *75*, 539−555. (d) Nicosia, R. F.; Lin, Y. J.; Hazelton, D.; Qian, X. Endogenous regulation of angiogenesis in the rat aorta model. Role of vascular endothelial growth factor. *Am. J. Pathol*. **1997**, *151*, 1379−1386.
(31) Ruggeri, B.; Singh, J.; Hudkins, R.; Gingrich, D.; Angeles, T.; Robinson, C.; Chang, H.; Hunter, K.; Dobrzanski, P.; Pritchard, S.; Vaught, J.; Dionne, C. CEP-7055: an orally-active VEGF-R kinase inhibitor with potent anti-angiogenic activity and antitumor efficacy against human tumor xenograft growth. *Proc. Am. Assoc. Cancer Res*. **2002**, *43*, 5347.
(32) Ruggeri, B. A.; Robinson, C.; Angeles, T.; Wilkinson, J.; Clapper, M. L. The chemopreventive agent Olipraz possesses potent antiangiogenic activity in vitro, ex vivo, and in vivo and inhibits tumor xenograph growth. *Clin. Cancer Res*. **2002**, *8*, 267−274.
(33) Rotin, D.; Margolis, B.; Mohammadi, M.; Daly, R. J.; Daum, G.; Li, N.; Fischer, E. F.; Burgess, W. H.; Ullrich, A.; Schlessinger, J. SH2 domains prevent tyrosine dephosphorylation of the EGF receptor: identification of Tyr992 as the high-affinity binding site for SH2 domains of phospholipase C-γ. *EMBO J*. **1992**, *11*, 559−567.

JM0301641